DEATH-ASSOCIATED PROTEIN KINASE REGULATES VASCULAR SMOOTH

MUSCLE CELL SIGNALING AND MIGRATION

Emily Keller Blue

Submitted to the faculty of the University Graduate School
in partial fulfillment of the requirements
for the degree
Doctor of Philosophy
in the Department of Cellular and Integrative Physiology,
Indiana University

December 2010

Accepted by the Faculty of Indiana University, in partial
fulfillment of the requirements for the degree of Doctor of Philosophy.

_____

Patricia J. Gallagher, Ph.D., Chair

_____

Jeffrey S. Elmendorf, Ph.D.

Doctoral Committee

_____

B. Paul Herring, Ph.D.

November 16, 2010

_____

Simon J. Rhodes, Ph.D.

_____

Debbie C. Thurmond, Ph.D.

Dedication

I would like to dedicate this dissertation to my mentor Patricia Gallagher; to my three boys, John, Ryan, and Cameron Blue; and to my parents, Jim and Pat Keller.

To Pat, you have given me support and encouragement when I needed it. You've been such a good example of a researcher, a teacher, a mentor, and a mother to your wonderful daughter Katya. And you also showed me how to fight when you need to. Thank you for giving me the freedom to learn on my own and make mistakes. For all that you've taught me, I dedicate this to you.

To my boys: John, you have been very understanding and supportive of me throughout the long years of research. Your love and patience are invaluable; I definitely could not have done this without you. To Ryan and Cameron, I know this work has taken me away from you, and I really appreciate your efforts at understanding. I also appreciate all the times you came to the lab with me, and hope you grow up with an appreciation for science and research, whatever you decide to do in your life.

To my parents, you provided me with so many opportunities to develop myself, and encouraged me to find what I really wanted to do (as long as I could support myself at it!) Thank you for all that you have done for me, and continue to do for us as a family. Go IU!

Acknowledgements

So many people have contributed to my education and development over my graduate studies, from the professors who taught my first- and second-year coursework, to coworkers and fellow students in and beyond this department. A few of them are listed here.

First and foremost, I have to thank my mentor, Dr. Patricia Gallagher. From the time she hired me to be a technician in her lab many years ago, she have always believed in me and supported me even when I doubted myself. Pat has been a wonderful mentor and a friend; I definitely share this accomplishment with her.

I also need to thank Dr. Paul Herring. Paul has been a second mentor to me, and I so appreciate all the time and effort you have made on my behalf, even when you probably did not have time to do it. I also thank the other members of my graduate committee who have encouraged and supported me through my graduate studies: Dr. Jeffrey Elmendorf, Dr. Simon Rhodes, and Dr. Debbie Thurmond. You have all given me thoughtful guidance and suggestions, and I really appreciate them, and have reflected on them often throughout this journey.

I would like to also thank the NIH and the Diabetes and Obesity T32 training program and the American Heart Association for supporting my research. I feel honored to have received these awards.

Several groups at IU and elsewhere also helped by supplying reagents, equipment, and essential protocols. Notably, I thank Dr. Cheikh Seye and Dr.

Scott Boswell for allowing me to use their Nucleofectors numerous times. Also, the Pavalko and Rhodes labs have always generously allowed me to use various pieces of equipment which contributed to the development of this dissertation. I also thank Dr. Keith March, Dr. Brian Johnstone, and Dr. David Ingram for supplying some of the mice used in my studies.

I also would like to thank current and former members of the Gallagher and Herring labs, especially Shelley Dixon, Ryan Widau, Liguo Zhang, April Hoggatt, Ketrija Touw, Rebekah Jones, Meng Chen, and Jury Kim. I have truly enjoyed getting to know all of you, and appreciate all the help you have give me, and the laughter we have shared over the years.

I also need to thank my parents and my husband John for their support throughout my graduate years. I truly could not have made it through this experience without you. Graduate school is difficult, especially with two young sons, and your help and support has been invaluable. Finally, I would like to thank my two sons, Ryan and Cameron. I know that my lab work took me away from you at times; I hope you understand that you are part of this achievement too.

Abstract

Emily Keller Blue

DEATH-ASSOCIATED PROTEIN KINASE REGULATES VASCULAR SMOOTH

MUSCLE CELL SIGNALING AND MIGRATION

Cardiovascular disease is the number one cause of death for Americans. New treatments are needed for serious conditions like atherosclerosis, as it can lead to stroke and heart attack. Many types of cells contribute to the progression of cardiovascular disease, including smooth muscle cells that comprise the middle layers of arteries. Inappropriate growth and migration of smooth muscle cells into the lumen of arteries has been implicated in vascular diseases. Death associated protein kinase (DAPK) is a protein that has been found to regulate the survival and migration of cancer cells, but has not been well characterized in vascular cells. The objective of this work was to determine the signaling pathways that DAPK regulates in smooth muscle cells.

These studies have focused on smooth muscle cells isolated from human coronary arteries (HCASM cells). We have determined that HCASM cells depleted of DAPK exhibit more rapid migration, showing that DAPK negatively regulates migration of vascular cells. Results from a focused RT-PCR array identified matrix metalloproteinase 9 (MMP9) as a gene that is increased in cells depleted of DAPK. MMP9 is an important enzyme that degrades collagen, a

component of the extracellular matrix through which smooth muscle cells migrate during atherosclerosis. We found that DAPK regulates phosphorylation of the NF-κB transcription factor p65 at serine 536, a modification previously found to correlate with increased nuclear levels and activity of p65. In DAPK-depleted HCASM cells, there was more phosphorylation of p65, which causes increased MMP9 promoter activity. Additional experiments were conducted using transgenic mice in which the DAPK gene has been deleted. By studying these mice, we have determined that under some circumstances DAPK augments maximal MMP9 levels in mouse carotid arteries which have been injured by ligation surgery via other signaling pathways.

MMP9 has been previously implicated as a protein that promotes vascular diseases such as atherosclerosis. Our research in identifying DAPK as a regulator of MMP9 expression identifies a new target for treatment of vascular diseases like atherosclerosis.

Patricia J. Gallagher Ph.D., Chair

Table of Contents

List of Tables

List of Figures

Abbreviations

ADAMTS8	A disintegrin and metalloproteinase with thrombospondin motifs 8
AP1	activator protein 1
ApoE	apolipoprotein E
BCA	bicinchoninic acid
bFGF	basic fibroblast growth factor
CaM	calmodulin
CaMKK	calcium/calmodulin-dependent protein kinase kinase 1
CHIP	C-terminal HSC70-interacting protein E3 ubiquitin ligase
CLEC3B	C-type lectin domain family 3, member B
CTGF	connective tissue growth factor
DAPK	death-associated protein kinase
DAPK KO	DAPK -/- or DAPK knockout
DAPK3	death-associated kinase 3
DMSO	dimethyl sulfoxide
Δneo	deletion of the neo cassette
DRAK1	DAPK-related apoptosis-inducing protein kinase 1
DRAK2	DAPK-related apoptosis-inducing protein kinase 2
DRK1	DAPK related kinase 1
E-cadherin	epithelial cadherin
ECM	extracellular matrix
EGF	epidermal growth factor
ERK	extracellular-signal regulated kinase
FCS	fetal calf serum
GAPDH	glyceraldehyde-3-phosphate dehydrogenase
GFP	green fluorescent protein
HCASMC	human coronary artery smooth muscle cells
HDAC3	histone deacetylase 3
HEK	human embryonic kidney
HPRT	hypoxanthine guanine phosphoribosyltransferase 1
IB	immunoblot
ICAM1	intercellular cell adhesion molecule 1
IκBα	inhibitor of kappa B alpha
IκK	IkB kinase
IL-18	interleukin 18
IL-1b	interleukin 1 beta
IL-4	interleukin 4
JNK	c-Jun kinase
LDL	low-density lipoproteins
LDLR	LDL receptor
MAPK	mitogen-activated protein kinase
MCM3	mini-chromosome maintenance complex component 3

MCP-1	monocyte chemoattractant protein 1
Mib1	mindbomb1
MIF	macrophage migration inhibitory factor
MLCK	myosin light chain kinase
MMP	matrix metalloproteinase
NF-κB	nuclear factor kappa B
p65 phosphoS536	p65 phosphorylated on serine 536
PARP	poly-ADP-ribose polymerase
PDGF	platelet-derived growth factor
PECAM1	platelet-endothelial cell adhesion molecule 1
PKC-θ	protein kinase C theta
PKD	protein kinase D
PP2A	protein phosphatase 2A
qRT-PCR	quantitative reverse transcription-PCR
RHD	Rel homology domain
RIPA	radio-immunoprecipitation assay
RPLP0	ribosomal phosphoprotein, large, P0
RSK	ribosomal protein S6 kinase
SDS-PAGE	sodium dodecyl sulfate-polyacrylamide gel electrophoresis
siRNA	small interfering RNA
SMC	smooth muscle cells
SMRT	silencing mediator for retinoid and thyroid hormone receptors
SP1	specificity protein 1
TAD	transcription activation domain
TGFβ	transforming growth factor beta
TIMP3	tissue inhibitor of metalloproteinase 3
TK	thymidine kinase
TNFα	tumor necrosis factor alpha
VCAM1	vascular cell adhesion molecule 1
VLDL	very low-density lipoproteins
WT	wild-type
ZIPK	zipper interacting protein kinase

Chapter I: Introduction

Cardiovascular disease is the number one cause of death in the United States. Diseases such as atherosclerosis and restenosis following angioplasty can lead to death due to myocardial infarction and stroke. The determination of new therapies to prevent or halt the progression of these diseases is essential. The goal of the studies described in this dissertation was to characterize the role of death-associated protein kinase (DAPK) in vascular disease. The results of the studies presented here contribute to the accumulating knowledge of proteins and pathways that regulate the progression of vascular disease.

Atherosclerosis: Roles of smooth muscle cells

Atherosclerosis is a disease that involves multiple cell types, including endothelial cells, macophages, lymphocytes, and smooth muscle cells (SMC) (80). Smooth muscle cells are known to play a key role in the development of atherosclerosis (reviewed in (31)). Even *in utero* at 36 weeks' gestation, pre-atherosclerotic lesions called eccentric intimal thickenings are found in human large arteries; these are present in nearly all humans by the age of 1 year (52, 111, 122). These thickened regions generally consist mainly of SMCs and proteoglycans produced by these cells (111). These thickenings are of interest because the regions of the arteries where they tend to occur correlates with regions where advanced atherosclerotic lesions are found later in life (110, 111). Thus, inappropriate proliferation of SMC likely have roles in the early genesis of vascular disease (31). These roles include lipid uptake, maintenance of macrophage survival in lesions, and secretion of cytokines, extracellular matrix, and proteases.

SMC have several different characteristics and roles that are thought to contribute to atherosclerosis. A change in phenotype can often occur when the cells are exposed to an atherogenic environment *in vivo* (18, 90). SMC exhibit a switch from a "contractile" phenotype to a "synthetic" phenotype, when the cells

are exposed to stimuli like altered extracellular matrix (11, 115), cytokines (29, 45, 77), shear stress (97), reactive oxygen species (113), and lipids (93). SMC are often exposed to such conditions during atherosclerosis, prompting the cells to decrease levels of smooth muscle contractile proteins like sm-α-actin, calponin, and smooth muscle myosin heavy chain, and to increase synthesis of collagen and other extracellular matrix proteins (90). The phenotypically "synthetic" cells also exhibit increased migration and proliferation. Inappropriate migration and proliferation of SMC has long been viewed a hallmark of vascular disease, and these altered, migratory and proliferative SMC likely contribute to the progression of atherosclerosis (90). In addition, receptors for VLDL and LDL increase during this phenotypic switch, leading to cholesterol uptake by SMC, turning these SMC into foam cells (75, 98, 101). *In vitro* culture models used in the studies in Chapter II allow for the addition and subtraction of growth factors to mimic the atherogenic stimuli that induce phenotypic switching.

SMC also play a role in the retention and survival of monocytes and macrophages in atherosclerotic lesions. Endothelial cells interact with monocytes as they are migrating into the intima, via expression of adhesion molecules like ICAM1 and VCAM1. These receptors are also expressed by SMC, and can mediate interactions with macrophages (12, 16, 112). Previous studies have found that VCAM1 and ICAM1 are expressed by intimal smooth muscle cells in human and mouse atherosclerotic coronary, aorta, and carotid arteries, but not in healthy medial smooth muscle (33, 57, 89). VCAM1 expression is found in lesion prone areas of arteries in the ApoE-/- mice, possibly indicating that its expression is important in the early generation of plaques (12). Blockade of VCAM1 with a neutralizing antibody leads to increased apoptosis of monocytes in a SMC-monocyte co-culture model, indicating that these adhesion receptors promote survival of monocytes *in vivo* (16). Other pathways can also lead to increased monocyte binding to SMC, resulting in prevention of apoptosis (15).

SMC also produce cytokines, extracellular matrix, and proteases which may be important in atherogenesis. SMC produce PDGF, TGFβ, macrophage

inhibitory factor (MIF), interferonγ, and monocyte chemoattractant protein (MCP-1) (4, 43, 84, 88, 92, 96). These cytokines, many of which are also produced by other cells in atherosclerotic plaques, can act in an autocrine fashion to induce ECM production. In addition, by acting in a paracrine fashion, many of these cytokines can induce endothelial dysfunction (96). SMC are the major producers of ECM in both healthy arteries and in atherosclerotic plaques (34). Type I and III collagen fibers make up the bulk of the ECM in healthy arteries; however, the atherosclerotic arteries contain increased proteoglycans, with some collagen I fibrils and fibronectin (99). This alteration in ECM allows atherosclerotic arteries to trap more LDL, leading to increased oxidized LDL, accelerated lesion progression, and cell proliferation (17, 19, 21). Also, the change from the fibrillar collagen found in healthy arteries to the proteoglycan and fibronectin rich plaques induces SMC to start proliferating; these proliferative SMC also increase production of proteoglycan, leading to increases in lesion size (17, 67, 100). Both SMC and macrophages produce matrix metalloproteinases; these will be discussed in the following section.

Matrix metalloproteinase 9 and atherosclerosis

Several matrix metalloproteinases are found upregulated in atherosclerotic lesions, including MMP1, MMP2, MMP3, MMP7, MMP8, MMP9, MMP11, MMP12, MMP13, MMP14, and MMP16 (86). MMP2 and MMP9 are the two gelatinases that are secreted by SMC. These proteases can degrade a variety of substrates, including gelatin, collagen, fibronectin, laminin, and versican. MMP9 can also degrade cytokines and chemokines, resulting in alteration of their activity (119). The importance of MMP9 in the regulation of smooth muscle cell migation has been well documented, both *in vitro* and *in vivo* (26, 38, 82). Incubation in conditioned media from rat aortic SMC overexpressing MMP9 led to increased SMC migration *in vitro* (82). Also, a study by Galis, et al. (2002) found that MMP9^{-/-} mice showed impaired SMC migration in response to ligation of the carotid artery (38, 62). Results presented in **Chapter II** show that DAPK

negatively regulates expression of MMP9 *in vitro* in primary vascular smooth muscle cells, and **Chapter III** shows that DAPK promotes MMP9 expression in an *in vivo* model. Tight regulation of MMP9 activity is important for maintainence of plaque stability. Expression of active MMP9 by macrophages resulted in plaque instability and disruption in ApoE$^{-/-}$ mice (41). This result implies that the role of DAPK as a regulator of MMP9 expression likely has important implications for vascular disease.

Mouse models of atherosclerosis and vascular disease

Several mouse models exist for the study of atherosclerosis and vascular disease. Although there are disadvantages to mouse models, using a mouse model has the advantage of enabling the use of a variety of transgenic and gene knockout models, which are not extensively available for other species. Unfortunately, unlike humans, mice do not spontaneously develop large atherosclerotic lesions; small lesions similar to human fatty streaks can be induced by a high-fat/high-cholesterol diet (91, 114). Knockout approaches in combination with altered diet and/or vascular surgery are used to induce atherogenesis in mice (1, 65). The two main models of mouse atherosclerosis are the ApoE$^{-/-}$ mouse, and the LDLR$^{-/-}$ mouse (55, 94, 95, 130). Both of these models exhibit marked increases in serum cholesterol, especially when the mice are fed a high fat/high cholesterol diet, which results in the formation of complex atherosclerotic lesions. The high fat/high cholesterol diet accelerates the formation of the atheromas (65). Thousands of studies have been done over the last two decades using these atherosclerotic mice.

Vascular surgery is another way to induce atherogenesis in mice and other rodents (126). Several models exist to mimic injuries induced by angioplasty, including carotid artery catheter injury and femoral artery wire injury (79, 105). In addition, the carotid artery ligation surgery mimics vascular changes that occur as a result of blockage of an artery, resulting in thrombosis and altered shear stress (69). These three models have slightly varied results, in the type of

cells predominantly contributing to the lesions, and in the response to injury, but all of them generally result in SMC proliferation and migration, resulting in a thickened medial smooth muscle layer, and often the formation of a neointimal layer (126). Thus, these are accepted ways to test SMC migration and proliferation *in vivo*. The carotid artery ligation model was used to test the *in vivo* role of DAPK in chapters II and III. Atherosclerotic lesions often occur in humans at sites with altered shear stress; thus, the carotid ligation model mimics this situation (68). In addition, MMP9 is upregulated rapidly in the mouse carotid injury model, enabling *in vivo* studies of factors regulating its expression (40). Studies using mice deficient in MMP9 have revealed the importance of this vascular protease in the response to vascular injury (62).

Regulation of MMP9 transcription and stability

The regulation of MMP9 transcription has been extensively studied in many cell types. As opposed to the constitutively expressed MMP2, the MMP9 gelatinase is induced in vascular smooth muscle cells by a variety of cytokines, including TNFα, IL-1β, IL-4, IL-18, PDGF, and bFGF (reviewed in (87)). The MMP9 promoter has several well-characterized *cis*-regulatory elements, shown in **Figure 1** including an AP1 binding site, an NF-κB binding site, and SP1 binding site (20, 76). The AP1, NF-κB, and SP1 binding sites are required for maximal MMP9 promoter activity in SMC and deletion of even one of these sites results in much lower induction of MMP9 by cytokines. In addition, steady-state levels of MMP9 can be regulated by signaling to stabilize the MMP9 mRNA, originating from α3β1 integrin (56). However, this regulation has not been verified in SMC.

NF-κB signaling: overview and role of phosphorylation

The NF-κB transcription factor family contains five members, p65/Rel A, Rel B, c-Rel, NF-κB1 p105/p50, and NFκ–B2 p100/p52 (reviewed in (23, 46, 85)). These proteins play important roles in a variety of cell processes, including apoptosis control, proliferation and differentiation. Specificity of signaling is

thought to occur via interaction of different combinations of homodimers and heterodimers, in conjunction with interactions with other transcription factors. While all the family members contain a Rel homology domain (RHD) required for DNA binding and dimerization, only the "Rel" proteins p65/RelA, Rel B, and cRel contain the transcription activation domain. Generally, heterodimers of one "Rel" protein (p65/RelA, RelB, or cRel) form with one non-TAD containing protein (p50 or p52). The translocation of the dimers to the nucleus is regulated by the binding of several inhibitors of NF-κB (IκB), which both promote the nuclear export of p65 and p50, and maintain p65/p50 and p65/p65 dimers in the cytosol. The canonical signaling involves activation that results in degradation of IκB induced by IκKβ, allowing the translocation of p65/p50 dimers to the nucleus to bind promoters and activate transcription(reviewed in (23, 46)). Other inhibitors of NF-κB signaling include the unprocessed, full-length NF-κB1 (p105) and NF-κB2 (p100). Cleavage of the inhibitory domains from p105 and p100 reveals the p50 and p52 "active" versions.

The regulation of NF-κB also involves phosphorylation and acetylation of the family members (reviewed in (51)). Several phosphorylation sites on p65 have been identified, and they exert a variety of effects that are still being characterized. Of interest to this dissertation is the phosphorylation of S536 on p65. This phosphorylated serine is located in the transactivation domain of p65, and has been reported to increase NF-κB activity. The mechanism behind this increase is likely to due to a conformation change that alters its interaction with other proteins. Notably, p65 phosphoS536 exhibits decreased affinity for IκB. This leads to an inability of IκB to export p65 phosphoS536 from the nucleus (10, 13, 39). In addition, p65 phosphoS536 has increased binding to the histone acetyltransferase p300, and decreased binding to the SMRT and HDAC3 co-repressors (24, 47). Several kinases can mediate this phosphorylation, including IκKα/β and RSK1(102, 103). Results presented in **Chapter II** reveal an indirect role for DAPK in regulation of p65 phosphorylation on S536.

Death-associated protein kinase

Death-associated protein kinase-1 (DAPK) is a 160-kD serine/threonine kinase. As its name implies, the human DAPK1 cDNA was originally cloned as a gene that contributes to interferon-γ induced cell death (30). At the same time, the Gallagher lab cloned the mouse DAPK1 cDNA based on the high degree of homology between kinase domain of DAPK and myosin light chain kinase (MLCK) (58). DAPK is part of a family of death-related kinases; other family members include DAPK-1-related protein 1 (DRK1 or DAPK2), zipper interacting kinase (ZIPK or DAPK3), DAP-kinase related apoptosis inducing protein kinase 1 (DRAK1) and DRAK2 (9). The kinases in this family do share highly similar kinase domains, but the other domains in these proteins give them unique functions *in vivo*. DAPK1 (referred to as DAPK in this dissertation) is the most well studied member of this family, and is the focus of the experiments described in the subsequent chapters.

DAPK has been implicated in a variety of cellular functions, including regulation of apoptosis, autophagy, survival, cell migration, and adhesion (9, 58, 61, 71, 121, 128). DAPK has been proposed to be a tumor suppressor, after findings indicated that methylation of the DAPK promoter was linked to cancer recurrence and metastasis (9). Many early studies linked the kinase activity of DAPK to the promotion of apoptosis and autophagy. However, many of these reports were performed using cells overexpressing a constitutively active form of DAPK which can induce morphological changes that cause cells to round and detach from the extracellular matrix (121). More current studies, using siRNA depletion of DAPK and other strategies, have identified non-death related roles for the protein (78).

DAPK has several domains that mediate protein-protein interactions with a variety of proteins. The domains include an N-terminal kinase domain, a calmodulin (CaM) binding domain, a series of eight ankyrin repeats, two P-loops, a cytoskeletal binding domain, and a death domain (**Figure 2**). Previous studies have found that the non-kinase domains are important in mediating interactions

7

with other proteins and also for regulation of kinase activity; in fact, most of the proteins that have been shown to bind to DAPK are not substrates of the kinase (78). The experiments in this dissertation used strategies such as siRNA knockdown and genetic ablation of DAPK to further examine the physiological role of DAPK in the smooth muscle cells of the vasculature. Thus, the focus was on deletion of the protein as a whole, and not specifically on the kinase activity, so only a few of the 11 substrates of DAPK will be highlighted here. First, DAPK is a substrate for itself and undergoes autophosphorylation at S308 (**Figure 2**). This phosphorylation site lies within the calmodulin binding region, and blocks activation of the kinase by inhibiting binding of the activator Ca2+/calmodulin to the region (60, 109). Dephosphorylation of this site by PP2A represents part of the mechanism by which DAPK is activated in response to detachment induced cell death, or anoikis (123). Another well-characterized substrate of DAPK is myosin regulatory light chain (MLC) and phosphorylation of MLC activates myosin II motor activity leading to force generation needed for cell migration, shape changes, and cell division (7, 28, 58). Other proposed substrates include beclin-1, CaMKK, MCM3, p21, p53, S6, syntaxin-1A, tropomyosin-1, and ZIPK (6, 36, 48, 107-109, 116, 128).

Many proteins that interact with DAPK have been identified. Relevant to this dissertation are actin, MCM3, Mib1, PP2A, ERK, PKD, and RSK and these interactions will be briefly discussed (2, 6, 7, 22, 27, 28, 59, 123).

Early studies linked DAPK and actin, after limited biochemical studies showed that DAPK co-fractionates with actin in a RIPA lysate pellet (28). In this study, treatment of cells with Latrunculin A to inhibit actin polymerization resulted in an increase in the soluble DAPK, although at least half of the DAPK was still insoluble, while most of the actin was solubilized by Latrunculin A. Also, immunofluorescence performed on cells transfected with GFP-DAPK showed that the exogenous protein localized to the cytoskeleton. From these experiments, it was inferred that DAPK is a cytoplasmic, actin-bound protein, and that a cytoplasmic region is required for this interaction (28). Data that will be

presented in **Chapter II** contradict this finding and suggest that some of the DAPK is present in the nucleus. Supporting this statement is the recent identification of a novel DAPK substrate, the nuclear protein mini-chromosome maintenance complex component 3 (MCM3) (6).

Two E3 ubiquitin ligases that interact with DAPK are DAPK-interacting protein 1/Mindbomb1 (Mib1) and Carboxyl terminus of HSC70-interacting protein (CHIP) (59, 129). Studies have characterized roles for these E3 ligases in regulation of DAPK levels via ubiquitination and proteasomal degradation; however, these ligases may also have other roles that involve interaction and targeting by DAPK binding.

DAPK has been proposed to be involved in the regulation of several signaling pathways, including MAPK family members ERK and JNK, and NF-κB based on interactions with proteins such as ERK, protein kinase D (PKD), and PKC-θ. Previous studies have found that DAPK and ERK can phosphorylate each other, and that DAPK activity blocks the nuclear translocation of ERK in 3T3 cells (22). DAPK can also promote oxidative stress-induced JNK activation in HEK293 cells, via phosphorylation of PKD (32). Finally, DAPK blocks nuclear accumulation of NF-κB family member p65/RelA in T cells through regulation of PKC-θ, in response to T cell receptor activation, but DAPK does not does affect NF-κB signaling in response to TNFα in T cells (27).

DAPK has been previously linked to atherosclerosis by two studies, which found increased DAPK in and around atherosclerotic lesions (81, 124). The goal of the studies presented in this dissertation was to characterize the role of DAPK in smooth muscle cells, and determine how its expression affects vascular pathology. Based on studies showing that DAPK is upregulated in atherosclerotic plaques, and can regulate cell migration, I propose that DAPK regulates SMC signaling and migration. Studies in **Chapter II** will examine the effect of siRNA depletion of DAPK from primary smooth muscle cells. **Chapter III** will explore the role of DAPK *in vivo,* using a newly produced DAPK KO mouse model.

Figure 1: MMP9 promoter *cis* regulatory elements.

The MMP9 promoter contains the following conserved *cis* elements: an NF–κB binding site (-600), an AP1 binding site (-73) and an SP1 binding site at (-48). Adapted from (20, 76).
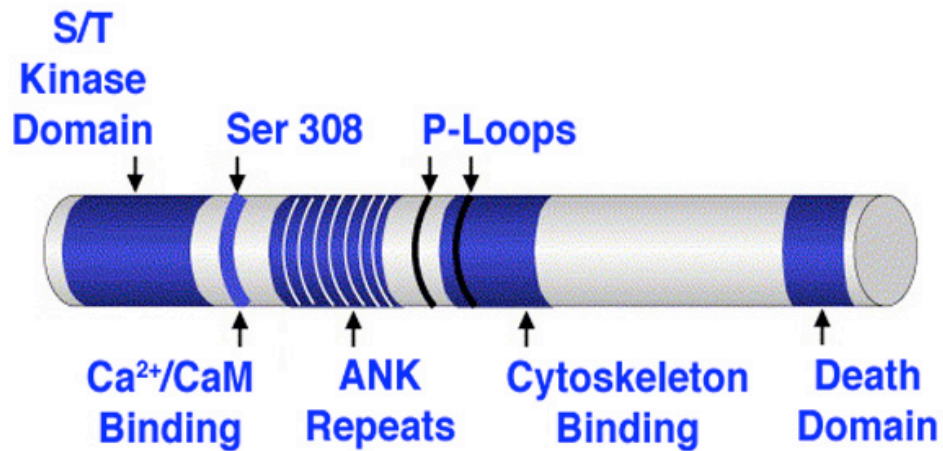
Figure 2: The domains of DAPK.

Schematic showing domains in DAPK, including the N-terminal ser/thr kinase domain, a Ca^{2+}/calmodulin binding domain which contains an auto-phosphorylation site at ser308, a series of 8 ankyrin repeats, 2 P-loops, a cytoskeletal-binding domain, and a death domain.

Chapter II: DAPK Blocks MMP9 Expression in Vascular Smooth Muscle Cells Via Indirect Regulation of NF-κB p65 Phosphorylation

Introduction

Inappropriate proliferation and migration of vascular smooth muscle cells contributes to the pathogenesis of many vascular diseases including atherosclerosis and restenosis (31). Many signaling pathways play a role in smooth muscle cell survival, migration, and proliferation, but our understanding of the regulation of these pathways is incomplete. Further knowledge of the regulation of these pathways will lead to better treatments of vascular disease.

Death-associated protein kinase 1 (DAPK or DAPK1) is a 160 kDa serine-threonine kinase which is regulated by Ca^{2+}/calmodulin binding (9, 58). Several studies have elucidated a role for DAPK in human cancers, and it has been proposed to be a tumor suppressor (64). DAPK overexpression can promote autophagy in some cells and also can regulate apoptosis (53, 128); the effect, however, is cell type and context dependent (8, 78). Several studies have also identified a role for DAPK as a negative regulator of cell adhesion and migration, however these studies have been performed in cancer cells and fibroblasts (70, 71, 121, 123). While DAPK is expressed in smooth muscle cells, and cell adhesion and migration are important roles of smooth muscle cells in the genesis of vascular disease, the role of DAPK in vascular smooth muscle cells has not been well studied. Two previous studies have identified increased levels of DAPK in regions of arteries containing atherosclerotic lesions (81, 124). However, these studies have not characterized the functional role of DAPK in vascular disease. Based on the previous work, we hypothesized that DAPK negatively regulates SMC migration.

In the current study, we used a focused RT-PCR based array to identify genes regulated by endogenous DAPK that could be regulating cell migration. This lead to the discovery that DAPK negatively regulates transcription of matrix

metalloproteinase 9 (MMP9) in primary smooth muscle cells via regulation of NF-κB family member p65.

Materials and Methods

Cells, Antibodies, and Reagents. Human coronary artery smooth muscle cells (HCASMC) are purchased from Lonza and were cultured as previously described (131). SMC growth media used was MCDB131 containing 5% FCS, 2 ng/ml human bFGF, 5 mg/ml human insulin, and 0.5 ng/ml human EGF. EGF, insulin, and bFGF were obtained from Invitrogen. HeLa cells were purchased from ATCC and were cultured in DMEM (Mediatech) containing 10% FCS and glutamine and penicillin/streptomycin (Mediatech). HeLa cells were transfected using Fugene 6 (Roche), following the manufacturer's protocol. Monoclonal antibodies to DAPK (clone 55), sm-α-actin (A2547), calponin (clone hCP) and vinculin were obtained from Sigma. Antibodies to MMP9, p65 phosphoS536, p65 phosphoS276, total p65, phospho-ERK, phospho-p38 MAPK, P- IκKα/β S176/S180, NF-κB1, NF-κB2, Rel B, and c-Rel were obtained from Cell Signaling Technology. GAPDH monoclonal antibody was purchased from Novus. Human DAPK siRNA was obtained from Dharmacon (D-004417-07) and p65/Rel A siRNA was purchased from Qiagen (SI00301672). The sequence of the double-stranded, nontargeting control siRNA was 5'-GAU GAC AGG UAU AGU AAG UUU-3', and was purchased from Dharmacon. TNFα, U0126, SP600125, and SB203580 inhibitors were purchased from EMD Biosciences. All other reagents were purchased from Fisher Scientific unless otherwise noted.

Nucleofections. Nucleofections were performed per the manufacturer's protocol for primary smooth muscle cells (Lonza, VPI-1004; Nucleofector II device). For Nucleofections of primary HCASMC, 80% confluent cells were trypsinized and pelleted. Each sample consisted of 1×10^6 cells and was resuspended in 100 μl of Nucleofection reagent and then mixed with either 4 μl 40 μM siRNA or 2-5 μg plasmid DNA. Cells were then nucleofected using program P-24. Cells were

immediately transferred to tubes containing SM-2 media (Lonza), and then cultured at 37°C in 5% CO_2 for 24-72 hours before analysis. Transfection efficiency was determined to be greater than 95% for siRNA using siGlo control siRNA (Dharmacon), and approximately 40% efficient for cDNA, as indicated by nucleofection of GFPmax cDNA (Lonza).

ApoE$^{-/-}$ mice. All animal studies followed the guidelines for care of animals at Indiana University and were approved by Indiana University IACUC. For the IHC studies, two-month old control, male C57BL/6 were obtained from Harlan and ApoE-/- mice were purchased from Jackson Laboratories. The mice were fed a Western diet containing 0.21% cholesterol and 21% fat (D12097B; Research Diets) for 3 months, anesthetized with a cocktail of ketamine (0.1 mg/g) and xylazine (0.01 mg/g), and aortas were harvested from the mice. For immunohistochemistry, mice were perfused with PBS and then by 4% paraformaldehyde in PBS. Aortas were fixed overnight in 4% paraformaldehyde, paraffin embedded, and sectioned. For RNA analysis, 6-month old ApoE$^{-/-}$ mice were obtained from both Jackson Laboratories and an internal colony of ApoE$^{-/-}$ mice, and were fed a Western diet for 2 months. The mice were anesthetized and perfused with PBS followed by RNAlater (Ambion). Aortas were stored in RNAlater at 4°C and then dissected under a dissection microscope, separating regions with white, visible plaques from plaque-free regions. Samples were frozen at -80°C, and RNA was prepared using Trizol after grinding tissue in a Pyrex glass tissue grinder.

Immunohistochemistry. Sections from paraffin-embedded aortas were rehydrated and antigens retrieved using a Retriever 2100 and R-Buffer UG (Electron Microscopy Services). Sections were stained with DAPK (1:75, Sigma, DAPK-55) and sm-α-actin (1:500, Sigma) antibodies overnight using the M.O.M. peroxidase kit and the NovaRed peroxidase substrate kit (both from Vector Laboratories). Negative controls included no primary antibody. Masson's

14

Trichrome staining was performed by the Indiana University Anatomy and Cell Biology Histology Core. Images were obtained from a Nikon Diaphot 200 microscope, and Olympus DP70 camera using Plan 10x Nikon objective and were compiled in Adobe Photoshop. All images were treated identically.

Carotid artery injury model. Eight-week old C57BL/6 mice underwent the carotid ligation surgery as previously described (69). Briefly, mice were anesthetized with a cocktail of ketamine (0.1 mg/g) and xylazine (0.01 mg/g). The carotid artery was exposed via a 0.5-cm incision 1-mm from the midline on the mouse's neck. A 4-0 silk suture was used to ligate the right common carotid artery, proximal to the bifurcation. Mice were sacrificed 4-14 days following injury, and the injured carotid artery rinsed in PBS and frozen in liquid nitrogen. Uninjured carotid arteries from mice that did not undergo surgery were used as controls. Lysates were prepared by grinding the frozen arteries in RIPA buffer containing protease and phosphatase inhibitors (Sigma) using a glass tissue homogenizer.

Migration assays. Modified Boyden chamber assays were performed by plating 50,000 cells per cell culture insert (8 μm pore size #353097; BD Biosciences). Inserts were placed in 24-well culture dishes containing MCDB131 plus 10% FCS in the lower well. After 6 hours of incubation, cells remaining on the upper side of the membrane were removed with a cotton swab, and migrated cells on the bottom side were fixed in 3.7% formaldehyde and stained with 0.4% crystal violet in 20% methanol. After briefly destaining in water, transwells were photographed and cells counted. Five fields were counted per transwell, and three transwells were used per condition for each experiment. Migration index was calculated by normalizing the number of cells migrated in test samples to cells migrated in control samples.

Superarray analysis. HCASMC nucleofected with control or DAPK siRNA were serum starved for 2 days in MCDB131 media. RNA was purified using Trizol and then treated with DNase I (Roche) to remove genomic DNA. cDNA for Superarray analysis was prepared using RT^2 First strand cDNA Synthesis Kit (SABiosciences). RT-PCR was performed RT^2 qPCR SYBR green Master Mix and the human Extracellular Matrix and Adhesion Molecules PCR Array (PAHS-013; SABiosciences). Data was analyzed using the SABiosciences protocol.

Real-time RT-PCR. RNA was prepared from cells or tissues using Trizol (Invitrogen). 0.5 μg was reverse transcribed as previously described (131). cDNA was diluted 1:5 with water, then amplified using Faststart SYBR green master mix (Roche) and gene specific primers (Eurofins MWG/Operon) in a AB 7500 Real-Time System (Applied Biosystems). Relative abundance of mRNA was calculated using the 2$^{-\Delta\Delta Ct}$ method. HPRT was used as an internal control for human RNA, and RPLPO was used as an internal control for mouse RNA. Primer sequences used are listed in **Table 1**.

Immunoblotting. Cells were lysed in RIPA lysis buffer containing protease inhibitor cocktail and phosphatase inhibitor cocktails 1 and 2 (Sigma). Protein was quantitated using a BCA assay (Pierce). Cytosolic and nuclear fractions were prepared using NE-PER Nuclear and Cytoplasmic Extraction Reagents (Pierce). Equal amounts of proteins were separated by SDS-PAGE, and detected using standard immunoblotting protocols. Immunoblots were imaged using a Syngene G-box and GeneSnap software (Synoptics). Quantitation of band intensity was performed using ImageJ (NIH).

Gelatin zymography. Zymography was performed as previously described with a few modifications (73). Briefly, to generate conditioned media, equal numbers of cells were plated in 6 well plates. Cells were serum starved in MCDB 131 (Mediatech) for 24 to 48 hours, and conditioned media was collected and

concentrated 50x using Ultracel-10K centrifugal filters (Amicon). Volumes of concentrated media were normalized to the amount of protein contained in the RIPA lysates, to compensate for variations in cell number. Media samples were separated by SDS-PAGE containing 7.5% acrylamide and 0.1% gelatin (BioRad). Gels were incubated in 2.5% Triton-X-100 for 30 minutes, then incubated in zymography buffer overnight at 37°C. (50 mM Tris pH 7.5, 200 mM NaCl, and 5 mM $CaCl_2$). Gels were stained in 0.5% Coomassie Blue R-250 in 7.5% methanol/7.5% acetic acid for 24 hours, followed by destaining in 7.5% methanol/7.5% acetic acid for 2 hours. Gels were dried and photographed using a Syngene GeneSnap imager.

Promoter assays. MMP9 promoter constructs (WT and mutAP-1) used in this study were the kind gift of Dr. Bysani Chandrasekar (University of Texas-San Antonio) (20), and were in pGL3b (Promega). The MMP9 mut-NF-κB construct was generated in this laboratory using site-directed mutagenesis of the NF-κB binding site using the Quikchange Site-Directed mutagenesis kit (Stratagene). Primers used were: forward (GGG GGT TGC CCC AGT GGC TTT TCA CAG CCT TGC CTA GCA G) and reverse (CTG CTA GGC AAG GCT GGA AAA GGC CAC TGG GGC AAC CCC C). The NF-κB-Luc plasmid was purchased from Stratagene. The p65 WT, S536A, and S536D mutant cDNAs were the kind gift of Dr. Carl Sasaki (NIH) (104). Primary HCASMC were Nucleofected with siRNA, and then plated and incubated at 37°C to allow siRNA to deplete target RNA. After 3 days, cells were Nucleofected again with MMP9 and NF-κB-luciferase cDNA constructs and plated in four wells of a 24-well plate in Lonza SM-2 growth media. One well was lysed in Laemli sample buffer and used to confirm protein expression and knockdown by immunoblotting. Three wells were lysed 18 hours after Nucleofection in Passive Lysis Buffer (Promega) containing protease inhibitor cocktail (Sigma), and assayed for Luciferase activity as previously described (131). Luciferase values were normalized to TK-Renilla (Promega).

Data analysis. All experiments were independently performed at least three times. All statistical analysis and graphs were created using GraphPad Prism software (GraphPad Software, San Diego, CA). Graphs display mean +/- sem of at least three independent experiments unless otherwise noted. Statistical significance was determined by Student's t test unless otherwise noted.

Results

To better understand the role of DAPK in vascular tissues, the expression pattern of DAPK in atherosclerotic lesions in the well-characterized ApoE$^{-/-}$ mouse model of atherosclerosis was examined. Paraffin sections of aortas from wild-type control and ApoE$^{-/-}$ mice fed a Western diet were stained for DAPK or sm-α-actin, and then examined for expression. **Figure 3A** shows a representative image from the aortas, revealing an increase in DAPK expression in the atherosclerotic plaque from the ApoE$^{-/-}$ mice, compared with the wild type control. Immunostaining of adjacent serial sections of atherosclerotic plaques shown in **Figure 3A** to detect expression of sm-α-actin, revealed that the areas of plaques with the greatest DAPK expression coincided this smooth muscle marker. Using RT-PCR the relative levels of DAPK mRNA were then quantitated in plaque versus non-plaque regions of aortas from ApoE$^{-/-}$ mice that had been fed a Western diet for 2 months. **Figure 3B** reveals that DAPK mRNA is significantly increased in plaque regions compared to non-plaque regions of the aortas. In addition to the atherosclerosis model, the carotid ligation model was also utilized to examining the expression of DAPK. Immunoblotting of tissue lysates from injured or uninjured control carotid arteries, revealed that DAPK protein was significantly upregulated as early as 4 days after injury, with peak levels observed by 7 days post-injury and this high level of expression was maintained for at least 2 weeks (**Figure 3C**). These data indicate that expression of DAPK is increased in two mouse models of vascular pathology and suggest a potential link to the development of vascular disease.

Smooth muscle cells are unique in that they can alter their phenotype depending on the conditions used to culture the cells (90). In the presence of serum and growth factors, the cells are more secretory, migratory, and proliferative, and they express less of the smooth muscle contractile proteins. Serum starvation induces a more differentiated state, with decreased secretion, migration and proliferation, and increased expression of smooth muscle marker proteins such as sm-α-actin, calponin, and sm22α. **Figure 4A** shows an immunoblot of lysates from primary human coronary artery smooth muscle cells cultured in either growth media, or serum-free media for up to 8 days. The results show that DAPK expression increased in parallel with the smooth muscle markers. This finding is consistent with our *in vivo* results, indicating that DAPK is expressed in more differentiated smooth muscle cells.

DAPK has been implicated in the regulation of cell migration in 3T3 fibroblasts and cancer cells (71). This observation prompted studies to determine whether DAPK regulates migration of smooth muscle cells. Nucleofection was used to introduce DAPK cDNA into the primary human coronary artery smooth muscle cells (HCASMC), and then the ability of these cells to migrate in a modified Boyden chamber assay was tested. As is seen in **Figure 4B**, overexpression of DAPK significantly reduced (43.0 +/- 8.0% of control) the ability of HCASMC to migrate toward the serum stimulus. Conversely, when Nucleofection of DAPK siRNA was used to deplete DAPK from the primary smooth muscle cells, the migration of primary HCASMC was augmented (**Figure 4C**; 45.4 +/- 11.3% increase over control). A representative immunoblot confirmed the overexpression of DAPK, and also shows that DAPK siRNA depletion was efficient (**Figure 4D**). These results indicate that DAPK is a negative regulator of smooth muscle cell migration.

DAPK has been shown to regulate many different cellular signaling pathways in other cell types, but the role in regulation of vascular smooth muscle migration is undefined. We hypothesized that alteration of DAPK protein levels in smooth muscle cells caused a change in signaling pathways, resulting in altered

transcription of downstream genes. A focused RT-PCR based screen of extracellular matrix and adhesion molecules was performed to identify genes related to cell migration that may be regulated by DAPK signaling, and ultimately the pathways DAPK impacts in primary smooth muscle cells. In this screen, the mRNA levels of extracellular matrix (ECM) and adhesion genes were compared in control and DAPK-depleted HCASMCs. Several genes were identified that were altered in response DAPK depletion including MMP9, E-cadherin, VCAM1, β3-integrin, PECAM1, TIMP3, ADAMTS8, CTGF, CLEC3B, and laminin α3. One of the targets, matrix metalloproteinase 9 (MMP9), a cytokine-inducible protease, was selected for further validation based on its link to cell migration and vascular pathology(87). In our screen, we found that MMP9 was increased 3.6-fold in HCASMC depleted of DAPK. In order to verify that MMP9 is increased in HCASMC, we examined MMP9 mRNA expression in HCASMC both in the presence and absence of serum. As is shown in **Figure 5A**, DAPK depletion leads to a 49.3 +/- 22.9% increase in MMP9 mRNA under growth conditions (plus serum and growth factors). The increase in MMP9 is more apparent in the serum-starved condition, when the absence of DAPK results in a 166 +/- 28% increase in MMP9 mRNA (**Figure 5A**). Under these conditions, we also validated a change in VCAM1, which was upregulated by 140 +/- 9% in DAPK-depleted cells in serum-free media, compared to control cells (**Figure 5B**). We also examined MMP9 protein levels in concentrated, conditioned media from HCASMC depleted of DAPK using both immunoblotting and gelatin zymography, which in-gel digestion of gelatin from MMP9 protein in samples results in light areas on a dark background after staining of the gel. The intensity of the light areas correlates with MMP9 levels in the conditioned media. This data revealed that depletion of DAPK in HCASMC caused an increase in the amount of MMP9 protein secreted (**Figure 5C**, lane 2). Conversely, overexpression of DAPK (**Figure 5C**, lane 3) suppressed MMP9 protein expression. Finally, rescue of DAPK expression by Nucleofection of DAPK cDNA in HCASMC previously depleted of DAPK, partially restored MMP9 secretion (**Figure 5C**, lane 4). Thus,

20

DAPK negatively regulates MMP9 mRNA and secreted MMP9 protein in HCASMC.

Previous reports have found that the steady-state levels of MMP9 mRNA can be altered by changes in the stability of the mRNA, involving signaling from integrin pathways (56). In order to determine if DAPK negatively regulates the stability of MMP9 mRNA in HCASMC, an RNA stability assay was performed. The mRNA levels of MMP9 were measured in control and DAPK-depleted HCASMC after treating the cells with the transcription inhibitor Actinomycin D for 8-24 hours. MMP9 mRNA levels were normalized to levels found in control cells treated in parallel with the vehicle, DMSO. As is shown in **Figure 5D**, there was no significant difference in the stability of MMP9 mRNA in control or DAPK-depleted HCASMC, either in growth conditions or in serum-free media. It is interesting to note that the presence of serum and growth factors did markedly stabilize MMP9 mRNA, with no degradation measured after 24h of Actinomycin D treatment (**Figure 5D**). Comparatively, HCASMC grown in the absence of serum exhibited a drastically reduced half-life of approximately 8 hours. Thus, while the presence of growth factors strongly stabilizes MMP9 mRNA, expression of DAPK does not affect the stability of MMP9 mRNA.

Since DAPK does not alter the stability of MMP9 mRNA, it likely acts by attenuating MMP9 promoter activity. MMP9 is an inducible gene that is regulated by cytokines via many signaling pathways in vascular smooth muscle cells, including the MAPK pathways (25). In order to determine if the increase in MMP9 that we observe in HCASMC depleted of DAPK is due to increased MAPK signaling, DAPK-depleted HCASMC were treated with inhibitors of ERK (U0126), JNK (SP600125) or p38 MAPK (SB203580), and the effect on MMP9 expression was measured by qRT-PCR. As is shown in **Figure 6A**, while DMSO-treated, DAPK-depleted HCASMC exhibited a 2.7-fold increase in MMP9 expression, this increase in MMP9 expression was not significantly affected by treatment of HCASMC with these MAPK inhibitors. Thus, the increase in MMP9 expression following DAPK depletion is not due to increased MAPK signaling.

In order to directly determine the effect of DAPK on the MMP9 promoter, promoter assays were performed using a previously described luciferase construct containing a 726-base pair region flanking the 5' end of the human MMP9 gene (20). This region of the MMP9 promoter is responsive to cytokines such as TNFα, and contains well-characterized *cis*-elements, which bind NF-κB and AP-1 transcription factors. Using Nucleofection to introduce the promoter construct into previously DAPK-depleted or control HCASMC, we found that DAPK depletion significantly increased MMP9 promoter activity (**Figure 6B**). To further determine the regulatory elements and pathways required for the DAPK effect, previously characterized promoter constructs containing point mutations at either the NF-κB binding site, or the AP-1 binding site were used. While mutation of the AP-1 binding site in the MMP9 promoter did not alter the effect of DAPK depletion, mutation of the NF-κB binding site blocked the effect of DAPK depletion on the MMP9 promoter (**Figure 6B**). Thus, the NF-κB binding site is required for the increase in MMP9 promoter activity observed when DAPK is depleted from HCASMC. As expected, the luciferase activities generated in response to the mutant AP-1 and mutant NF-κB sites were much lower than those generated from the wild-type MMP9 constructs, although they have detectable activity above empty pGL3b controls (data not shown). In addition, we directly tested the effect of DAPK on activation of a synthetic luciferase construct whose expression is driven by consensus κB binding elements. The NF-κB-Luc construct exhibited greater activation in HCASMC depleted of DAPK (**Figure 6B**). Thus, DAPK negatively regulates MMP9 expression via decreased NF-κB signaling.

The NF-κB signaling pathway is composed of 5 main family members: p65/Rel A, Rel B, c-Rel, NF-κB1 p105/p50, and NF–κB2 p100/p52. They form homodimers and heterodimers to activate transcription (23, 46). Much of the regulation of canonical NF-κB signaling occurs via maintenance of p65 in the cytosol by binding of inhibitors, such as IκBα. Upon stimulation, the inhibitors are

phosphorylated by IκKβ and degraded, allowing p65/p65 and p65/p50 dimers to translocate to the nucleus to activate transcription on NF-κB responsive genes. As the increase in MMP9 promoter activity was observed only when NF-κB binding site was intact, the possibility that DAPK might be altering the amount of p65 in the nucleus under basal conditions was examined. For this experiment, the levels of p65 in cytosolic and nuclear fractions from control and DAPK-depleted HCASMC were determined by immunoblotting. These results showed the expected increase in nuclear p65 in response to TNFα treatment (**Figure 7**, lanes 5 and 6); however, there was no significant difference in nuclear p65 levels following TNFα stimulation in control compared to DAPK-depleted cells (**Figure 7**, lanes 6 and 8). In addition, there was no difference in nuclear p65 under basal conditions (**Figure 7**, lanes 5 and 7). Finally, there were no changes in the levels of NF-κB1, NF-κB2, RelB, and c-Rel either in the cytosol or nuclear fractions (**Figure 7**). Interestingly, DAPK was predominantly found to be localized to nuclear fractions in control siRNA-treated HCASMC (**Figure 7**), although the significance of this finding is unclear.

Recently, the importance of post-translational modification of NF-κB-p65 (p65) has become appreciated (51). One site that has been shown to be important in the regulation of p65 localization and transcriptional activity is serine 536 (24, 47, 49, 102, 103). After finding that there was no change in the amount of total p65 in the nucleus, the amount of phosphorylated-S536 p65 (p65 phosphoS536) in control and DAPK-depleted cells was determined using a p65 antibody that specifically recognizes p65 phosphoS536 (**Figure 8A**). This experiment showed that a 44 +/- 16% increase in phosphorylation at p65 phosphoS536 was detected in HCASMC depleted of DAPK (**Figure 8B**). These results suggest that DAPK negatively regulates the phosphorylation of p65 at serine 536.

Some previous studies have suggested that p65 phosphoS536 increases the propensity for p65 to be retained in the nucleus (10, 13). Others suggest that p65 phosphoS536 alters the transcriptional activity of NF-κB, since S536 is

located within the transactivation domain of p65 (24, 47). To determine the effect of p65 phosphoS536 in primary HCASMC, these cells were first depleted of endogenous p65 by transfection with siRNA specific to p65. Subsequently, the p65-depleted cells were transfected with vectors for expression of wild-type p65, the phosphomimetic mutant, p65-S536D (serine to aspartic acid mutation) or the nonphosphorylatable mutant, p65-S536A (serine to alanine mutation). The effect of these transfected p65 proteins on a co-transfected NF-κB-Luc construct was then determined. As shown in **Figure 9A**, siRNA depletion of p65 was efficient in decreasing in NF-κB dependent promoter activity (approximately 50% decrease), which could be rescued by expression of wild-type p65 or the nonphosphorylatable mutant. The phosphomimetic mutant, p65-S536D showed 50% more NF-κB activity. These results indicate that S536 phosphorylation makes an important contribution to NF-κB transcriptional activity in primary HCASMC. Western immunoblotting confirmed that p65 was efficiently depleted from HCASMC (approximate 75% decrease) and that the relative expression levels of the transfected p65 wild type or mutant constructs while low, were similar (**Figure 9B**). Because the expression of the rescued protein was near the limit of detection in HCASMC, the expression levels of the constructs was also verified in HeLa cells and found to be similar (**Figure 9C**).

Based on the collective findings that DAPK depletion from HCASMC does not alter the level of nuclear p65 (**Figure 7**), increases the level of p65 phospho-S536 (**Figure 8**), and that p65 phosphoS536 enhances NF-κB activity (**Figure 9**), the relative levels of TNFα-stimulated p65 phosphoS536 in the nucleus following DAPK depletion were determined. These results revealed that there is a two-fold increase in the amount of TNFα-stimulated nuclear p65 phosphoS536 in DAPK-depleted cells, as compared with control cells (**Figure 10A**, lanes 6 and 8). Thus, although DAPK depletion does not change the amount of total p65 translocated to the nucleus, it does result in an increase in p65 phosphoS536. It should be noted that in the absence of TNFα stimulation nuclear p65 phosphoS536 is not detectable.

This data indicates that phosphorylation of p65 at S536 may have a role in regulating the amount of nuclear p65 available to activate transcription of genes like MMP9, and that DAPK regulates this phosphorylation. To determine if p65 expression was required for the increased NF-κB binding and increased MMP9 promoter activity observed in the DAPK-depleted HCASMC, siRNA was used to deplete endogenous DAPK and/or p65 from HCASMC. The effects of these depletions on NF-κB-regulated MMP9 promoter activity were measured using luciferase reporter assays. In these experiments, the results were normalized to either control siRNA alone, or p65 siRNA alone to specifically determine whether or not p65 was required for the increased activity observed when DAPK is depleted. As is shown in **Figure 10B**, depletion of DAPK led to an increase in the NF-κB promoter activity and this effect was attenuated when both p65 and DAPK were depleted from HCASMC. A similar trend was observed with the MMP9 promoter; DAPK depletion resulted in a slight increase in promoter activity, and the increase was blocked when both DAPK and p65 were depleted (**Figure 10B**). These results indicate that the increase in MMP9 promoter activity observed when DAPK is depleted from primary HCASMC likely requires p65, and probably occurs in response to increased phosphorylation of p65 at S536.

The increase in phosphorylation observed could be due to increased kinase activity by IκKα/β, which are known to phosphorylate p65 at S536. However, immunoblotting (**Figure 10C**) for the activated, phosphorylated IκKα/β was not different between control and DAPK depleted HCASMC, indicating that the p65 phosphoS536 is increased by another unknown mechanism.

Discussion

While previous studies have enhanced our understanding of the pathways regulated by DAPK and potential substrates for this protein kinase, these studies have focused on examining the role of DAPK in cancer cells, fibroblasts, and immune cells (22, 27, 32, 58, 71). The results presented here are unique in that they are the first to characterize the role of DAPK in primary vascular smooth

muscle cells. Using a focused RT-PCR based array, we have found that DAPK is a negative regulator of several genes linked to migration and extracellular matrix composition, including MMP9. The current study focused on the role of DAPK in regulation of MMP9, and our results demonstrated that there is a diminished secretion of MMP9 protein when DAPK is overexpressed, and enhanced MMP9 protein and mRNA when DAPK is depleted from primary HCASMC. Mechanistically these studies show that DAPK mediates its transcriptional regulation by blocking NF-κB activity. This finding is supported by results showing that mutation of a *cis* element in the MMP9 promoter that binds NF-κB blocks the effect of DAPK on this promoter. In addition, DAPK depletion from HCASMC results in increased nuclear p65 phosphoS536, while total levels of nuclear p65 are unchanged by DAPK depletion. Finally, we determined that NF-κB p65 is required for the increase in NF-κB activity observed when DAPK is depleted from HCASMC, since depletion of p65 from the cells blocked the DAPK effect.

Our studies confirm that DAPK mRNA and protein is upregulated in mouse atherosclerotic lesions particularly in sm-α-actin expressing cells within the plaques. Additionally we demonstrate that DAPK expression is also upregulated in the carotid ligation injury model at 4-14 days post-ligation. This data together with the finding that DAPK has an inhibitory role in HCASMC migration and the known role of DAPK in cancer cell and fibroblast migration suggests that DAPK may be important for regulation of SMC migration *in vivo*, a critical element in the development of many vascular pathologies (54, 71). Several genes including MMP9 that are important for cellular migration and ECM formation were altered in response to depletion of DAPK from HCASMCs. The finding that depletion of DAPK enhances HCASMC migration, together with the central role of MMP9 in VSMC migration and the development of atherosclerosis led to further examination of the potential role of DAPK in regulating the expression of this molecule (26, 38, 62, 74, 87).

Although the stability of MMP9 mRNA is unaffected by DAPK expression, total mRNA and protein levels are significantly altered, linking DAPK to transcriptional regulation of MMP9. Supporting this, MMP9 promoter activity was directly related to expression of DAPK. Several signaling pathways modulate expression of MMP9 including MAPK and NF-κB. Interestingly, while DAPK-depletion had no effect on the activation of MAPK pathways in primary HCASMC, it did significantly alter NF-κB signaling. The finding that depletion of DAPK did not alter MAPK signaling was surprising, since DAPK had been previously shown to block the nuclear translocation of ERK, and to be required for JNK activation under at least some conditions (22, 32). Despite the fact that a statistically significant change in MMP9 expression was not observed when DAPK-depleted cells were treated with the MEK inhibitor U0126, there was a trend toward a decrease in MMP9 mRNA levels, suggesting that ERK activation may make a minor contribution to the increased MMP9 promoter activity observed in DAPK-depleted cells. Relevant to this finding, a previous study utilizing aortic SMC demonstrated that ERK was required for maximal NF-κB activation and MMP9 expression in response to TNFα (83), so it is possible that ERK may be acting upstream of NF-κB in HCASMC.

Previously, Chuang et al. linked DAPK to negative regulation of NF-κB signaling in T cells, and in this study DAPK was found to block nuclear translocation of p65 in response to T cell activation (27). Although our results did not show any alteration in nuclear translocation of p65, DAPK depletion resulted in a significant increase in nuclear p65 phosphoS536. This suggests that the mechanism utilized by DAPK to regulate T cell signaling is likely very different than that used in HCASMC. Consistent with this is the additional finding that the T cell signaling response requires an atypical protein kinase C isoform, PKC-θ. Another difference between these two cell types is the partial membrane-association of DAPK in T cells, which clearly differs from our finding that DAPK is predominantly localized to the nucleus in HCASMC. This is another unanticipated finding, as it was previously reported that DAPK was predominantly found in the

cytoplasm, bound to actin filaments (28). Determining the localization of endogenous DAPK has been difficult in previous studies, as the available antibodies to DAPK are not suitable for immunofluorescent staining. Most, if not all, studies have relied on overexpression to visualize location of DAPK in the cell (7, 28). One previous study Cohen el al. suggested that DAPK localized with actin-containing insoluble fractions (28). It is possible that DAPK actually associates with DAPK with insoluble chromatin, which co-fractionated with actin in RIPA lysis buffer (28). Using a different cell fractionation protocol, we have found DAPK in the nucleus of several cell types, including HeLa and HEK293 (data not shown), suggesting that the localization of DAPK to the nucleus is not necessarily cell type dependent.

The increased level of nuclear p65 phosphoS536 when DAPK is depleted from HCASMC is an intriguing finding that can account for increased MMP9 expression. This proposal is supported by the fact that no other alterations in NF-κB family members were observed and because depletion of p65 resulted in blocking the DAPK effect on the MMP9 promoter. Thus, enhanced levels of nuclear p65 phosphoS536 is likely the reason for the observed increased NF-κB activity and MMP9 expression when DAPK is depleted from SMC. The NF-κB family member p65 can be phosphorylated on several different sites, and the roles of these phosphorylations are still being characterized (51). However, previous studies have determined that p65 phosphoS536 increases transactivation activity in luciferase assays (50), in agreement with our results in primary HCASMC. These previous studies have found that p65 phosphoS536 can both dissociate repressors such as SMRT and HDAC3 from promoters, and recruit p300/CBP activators to promoters (24, 47). In addition, phosphorylation of serine 536 also may alter the localization of p65, as it reduces the ability of p65 to bind to IκBα, thus allowing p65 phosphoS536 to resist nuclear export (10, 13, 39).

Several kinases are known to phosphorylate p65 on serine 536, including IκKα/β and RSK1 (102, 103). The finding that there is a significant increase in

p65 phosphoS536 when DAPK was depleted argues against the possibility that DAPK plays a direct role in phosphorylation of p65 at this site, even though it is a ser/thr kinase. In addition, examination of the p65 sequence did not reveal any sequences with similarity to other DAPK consensus phosphorylation site sequences (78, 106, 120). Since we observed an increase in p65 phosphoS536 in DAPK-depleted cells, we hypothesized that DAPK was negatively regulating one of these kinases. However, we found no changes in the active, phosphorylated forms of IκKα/β in DAPK-depleted HCASMC, either in the basal state, or following TNFα-activation (**Figure 10C**). In addition, parthenolide, an inhibitor of IκKα/β, had no signficant effect on the increased levels of MMP9 observed in DAPK-depleted cells (data not shown). These results led us to hypothesize about other mechanisms for regulating phosphorylation of p65, including phosphatase activity. One possibility is that PP2A, a known p65 phosphatase (127) which was recently shown to physically interact with DAPK (123), is not effectively targeted to p65 in DAPK-depleted cells. This alternative suggests the existence of a complex of proteins including DAPK, PP2A and p65 exists in cells; further studies will be required to validate this possibility.

Collectively, this report details a novel mechanism for regulation of VSMC migration that is modulated by the cellular levels of DAPK. DAPK appears to act upstream of NF-κB signaling and ultimately alters the level of p65 phosphoS536. Reduced DAPK expression enhances the levels of p65 phosphoS536 leading to increased MMP9 expression and increased VSMC migration. Current studies are focused on identifying the direct target of DAPK in the NF-κB signaling pathway and identifying additional transcriptional targets that are modulated by DAPK activity.
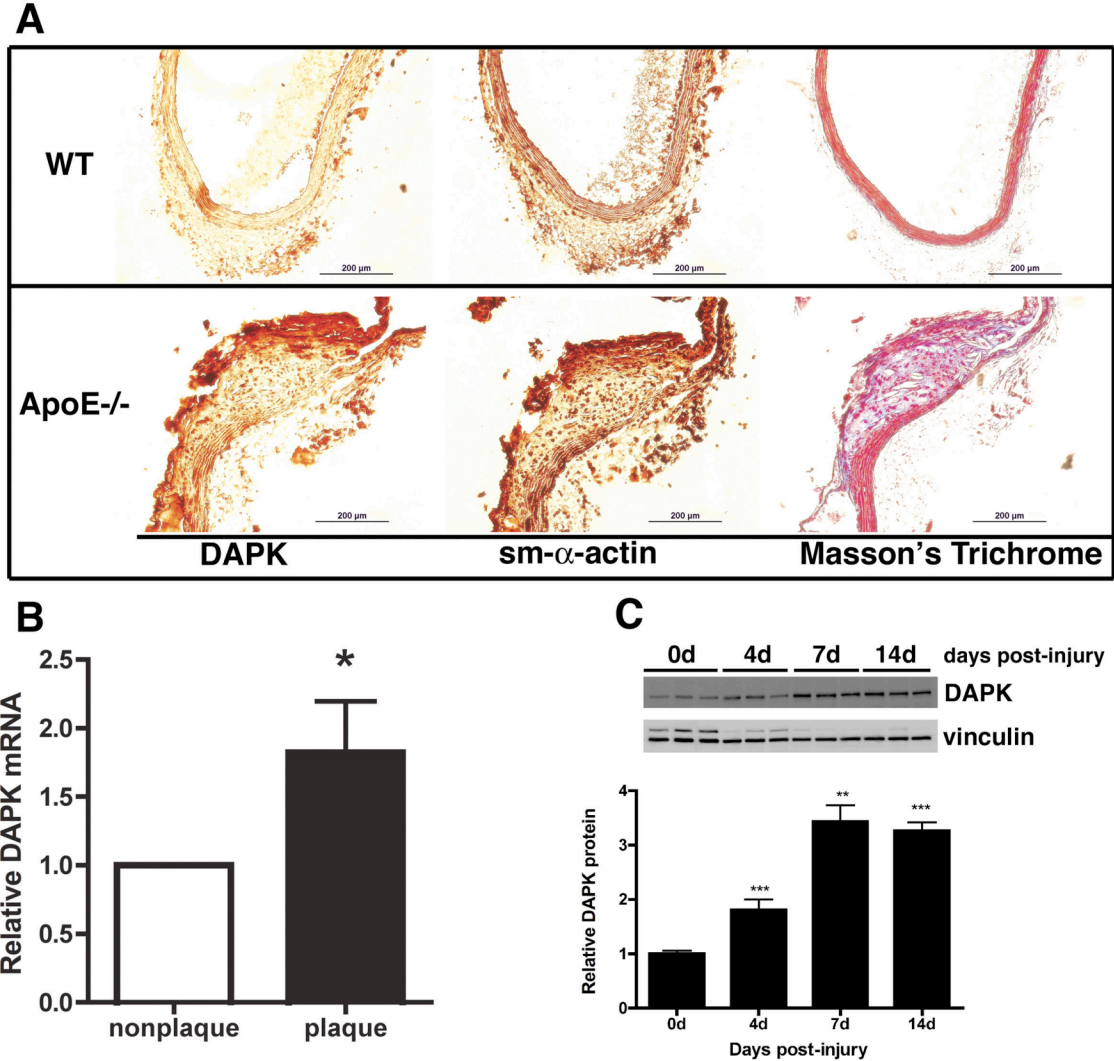
Figure 3: DAPK is upregulated in atherosclerosis and in response to vascular injury.

A: Paraffin sections from the aortas of ApoE^{-/-} and wild-type C57BL/6 mice (WT) that had been fed a Western diet for 3 months were stained to detect expression of DAPK or sm-α-actin. Brownish red staining represents areas of expression of DAPK or sm-α-actin. Histological staining with Masson's Trichrome stain is also shown; red staining indicates cytoplasm and blue staining indicates collagen. B: qRT-PCR was performed on RNA isolated from nonplaque or plaque regions of aortas from ApoE-/- mice fed a Western diet for 2 months. RPLP0 was used as the endogenous control. The mRNA levels in plaque regions were normalized to

its own nonplaque control for each mouse aorta, and a paired t test was used to compare samples. * $p<0.05$; n=13 per group. C: Immunoblotting of RIPA lysates (20 μg/lane) from ligated carotid arteries was performed. Vinculin was used as a loading control. The graph shows quantitation of DAPK protein, normalized to vinculin. T tests were used to determine statistical significance, compared to uninjured arteries (0 d). ***$p<0.001$; ** $p<0.01$; n=3.
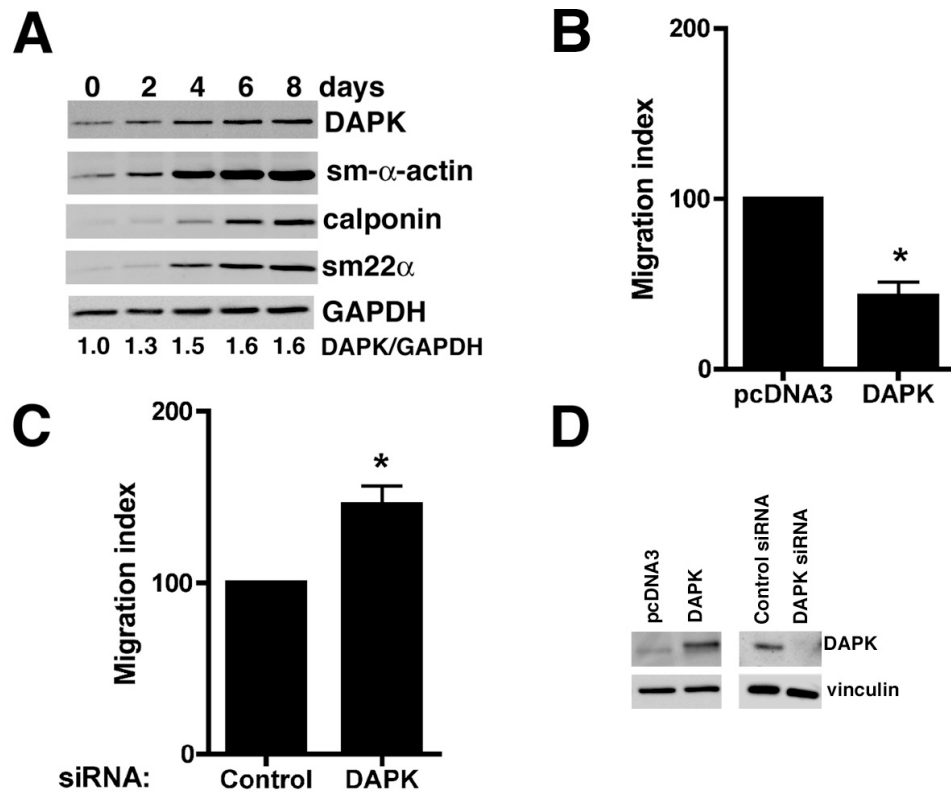
Figure 4: DAPK negatively regulates HCASMC migration.

A: Immunoblotting was performed on RIPA lysates from HCASMC that were serum-starved for 0-8 days to induce smooth muscle differentiation markers. Each lane represents 10 μg total protein, which was immunoblotted as indicated. DAPK levels were quantitated and normalized to GAPDH, as shown below blots. B & C: Modified Boyden chamber assays were performed using HCASMC that had been grown in serum-containing growth media. Upper well contained cells in serum-free medium, and lower well contained 10% FCS. Migrated cells were quantitated after 6 hours. Migrated cells in test samples normalized to control for each experiment. B: Two days before migration study, HCASMC were Nucleofected with either pcDNA3 or pcDNA3 DAPK construct. Results show mean +/- sem for three independent experiments. *P<0.05 by t test. C: Three days before migration study, HCASMC were Nucleofected with either control or DAPK siRNA. Results show mean +/- sem for five independent experiments. *P<0.05 by t test. D: Immunoblotting of lysates from parallel wells of HCASMC

used in migration studies showing overexpression of DAPK (left) and siRNA depletion of DAPK (right). Vinculin was used as a loading control.
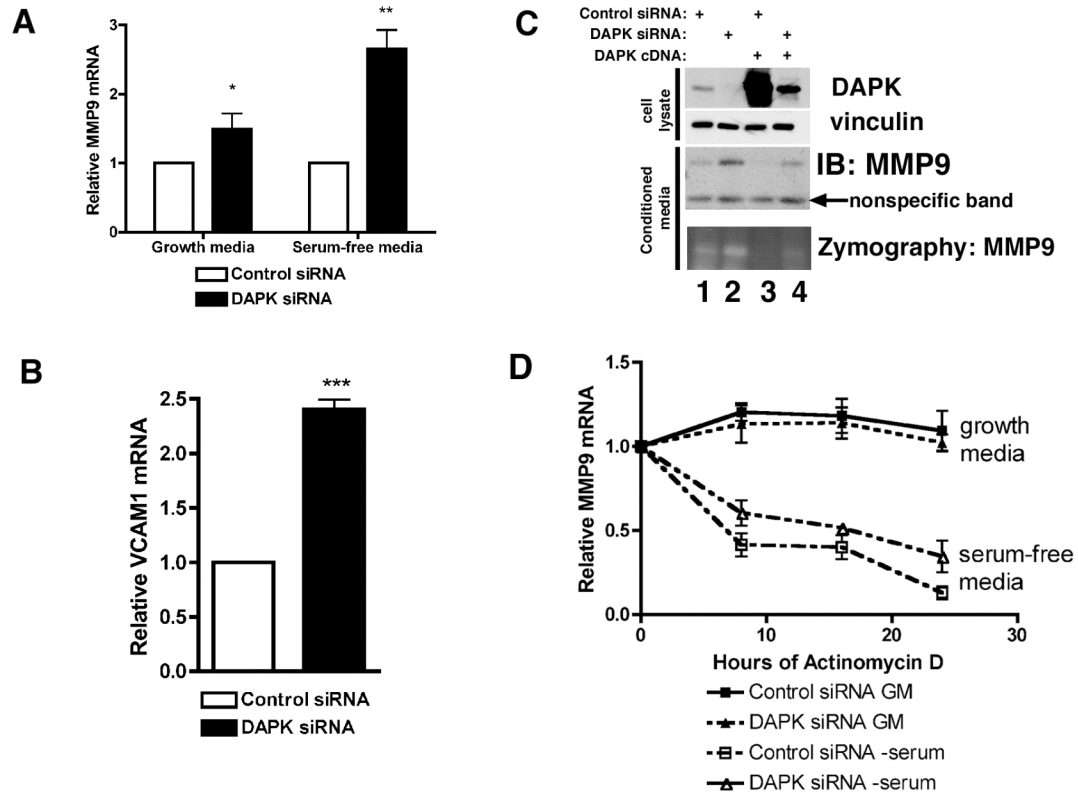
Figure 5: DAPK negatively regulates MMP9 and VCAM1 expression.

A: qRT-PCR was performed using cDNA from control or DAPK siRNA treated HCASMC with primers specific for MMP9. Growth media: cells were grown for 2 days in growth media before RNA was collected. HPRT was used as the endogenous control. Results show mean +/- sem for three independent experiments. Serum-free media: cells were grown in growth media for 2 days, followed by serum-free media for 3 days. Results show mean +/- sem for three independent experiments. *$p < 0.05$, **$p < 0.01$. B: qRT-PCR was performed for VCAM1 as described in A, using serum-free media. Results show mean +/- sem for four independent experiments. ***$p < 0.001$. C: Upper panels show immunoblots of RIPA lysates. Equal amounts of RIPA lysates from HCASMC were immunoblotted for DAPK and vinculin (loading control). Lower panels show immunoblot and gelatin zymography to measure relative MMP9 levels in conditioned media. Arrow denotes nonspecific band recognized by MMP9 antibody. D: mRNA stability assay for MMP9. DAPK or control siRNA were

introduced into HCASMC by Nucleofection. After 3 days, the Nucleofected HCASMC in growth media were treated with either carrier (DMSO, 0.1%) or Actinomycin D (4 μM) for 8-24 hours. For serum-free media samples, HCASMC were serum-starved for 3 days prior to addition of DMSO or Actinomycin D. qRT-PCR was performed on cDNAs generated, and MMP9 mRNA values were normalized to DMSO controls at each time point. The number of samples analyzed for each time point, n=3.
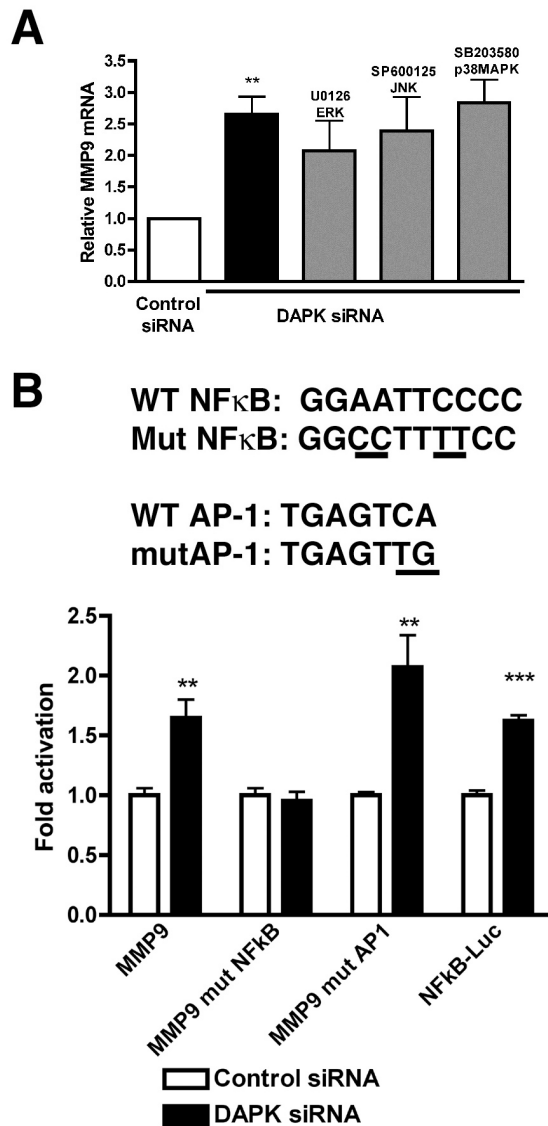
Figure 6: DAPK regulates MMP9 promoter activity by attenuating NF-kB activity.

A: HCASMC were Nucleofected with control or DAPK siRNA. Two days after Nucleofection, serum-free media was added and cells were incubated for two days. Cells were treated with DMSO (0.1%), MEK1 inhibitor U0126 (5 μM), JNK inhibitor SP600125 (10 μM), or p38MAPK inhibitor SB203580 (5 μM) for 24 hours, then RNA was collected, and cDNA generated. MMP9 mRNA was normalized to HPRT. Graph shows mean +/- sem for 4-6 independent experiments. **$p<0.01$. B: Upper panel shows sequence of wild-type and mutant

versions of plasmids used for MMP9 Luciferase constructs containing mutations in the NF-kB- and AP-1-binding sites of the human MMP9 promoter. HCASMC were Nucleofected with control or DAPK siRNA. After three days cells were Nucleofected a second time to introduce Luciferase constructs (2 μg pGL3b MMP9 or NFkB-Luc and 0.5 μg pTK Renilla). Cells were plated in triplicate in growth media. Each sample was normalized to Renilla to control for transfection variation, and DAPK siRNA normalized to control siRNA treated cells for each luciferase construct to calculate fold activation. Graph shows mean +/- sem for 3 independent experiments. ***$p < 0.001$, **$p < 0.01$.
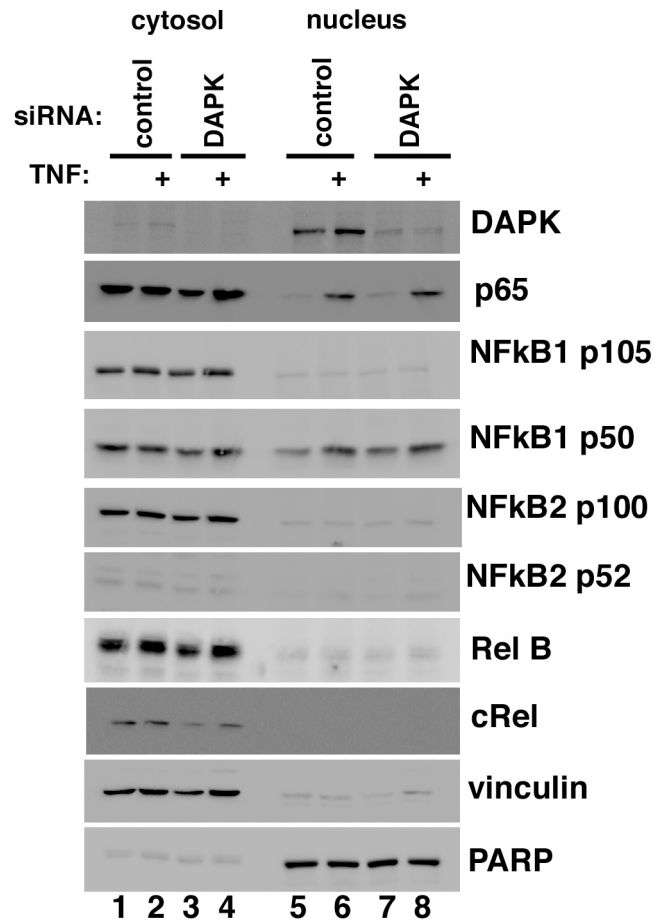
Figure 7: DAPK depletion does not alter p65 translocation to the nucleus.

Primary HCASMC containing either control or DAPK siRNA were serum-starved for 18 hours. TNFα (10 ng/ml) was added as indicated for 15 minutes. Nuclear and cytosolic fractions were isolated, and equal amounts of protein were analyzed by immunoblotting as indicated. Vinculin and PARP are included as cystosolic and nuclear markers, respectively. The levels of nuclear p65 did not significantly vary between cells expressing DAPK and those depleted of DAPK. Immunoblots are representative of three independent experiments.
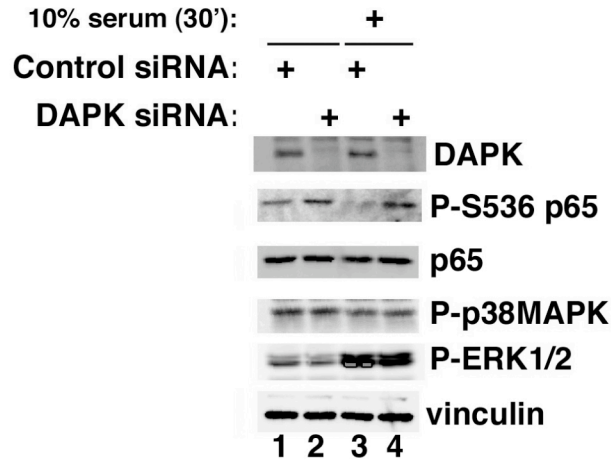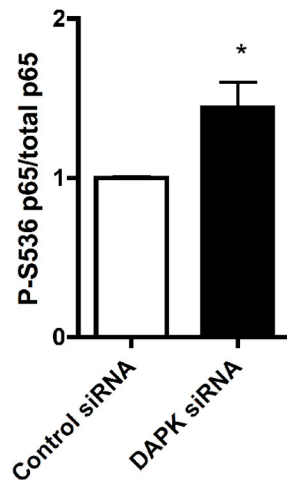
A

B

Figure 8: DAPK depletion increases p65 phosphoS536.

A: Representative immunoblot of RIPA lysates from HCASMC after depletion of DAPK with siRNA. HCASMC were Nucleofected with control or DAPK siRNA. Cells were serum-starved for 3 days, and then stimulated with 10% FCS for 30 minutes. RIPA lysates were collected and equal amounts of protein were immunoblotted as indicated. B: Quantification of p65 phosphoS536, normalized to total p65. Graph shows mean +/- sem for 6 independent experiments. *p<0.05 by t test.
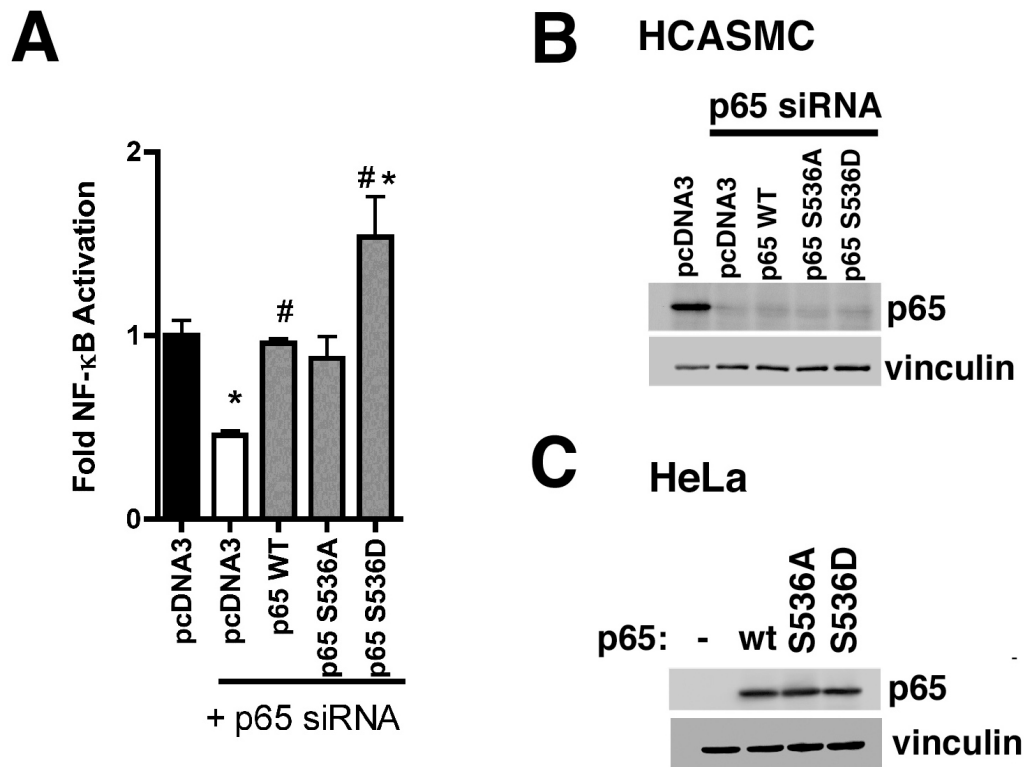
Figure 9: Phosphorylation of p65 at S536 increases activation of NF-κB.

A: HCASMC were Nucleofected with control or p65 siRNA. Three days later the cells were Nucleofected again with NF-κB-Luc (2 μg), pTK-Renilla (0.5 μg), and either pcDNA3, p65 WT, p65 S536A, or p65 S536D (2 μg) and cells were plated in growth medium. Luciferase assays were performed 18h after Nucleofection, measuring duplicate samples in triplicate wells. Fold NF-κB activation was determined by normalizing to control siRNA sample. Data is presented as mean +/- sem for triplicate wells a single experiment. *$p<0.05$ vs. pcDNA3/control siRNA (column 1); #$p<0.05$ vs. pcDNA3/p65 siRNA (column 2). Similar results were obtained in three independent experiments. B: Immunoblotting of HCASMC lysates from p65 siRNA/p65 rescue experiment in parallel wells Nucleofected in A. C: Immunoblotting of HeLa lysates transfected with p65 constructs used in A and B. Vinculin is used as a loading control.
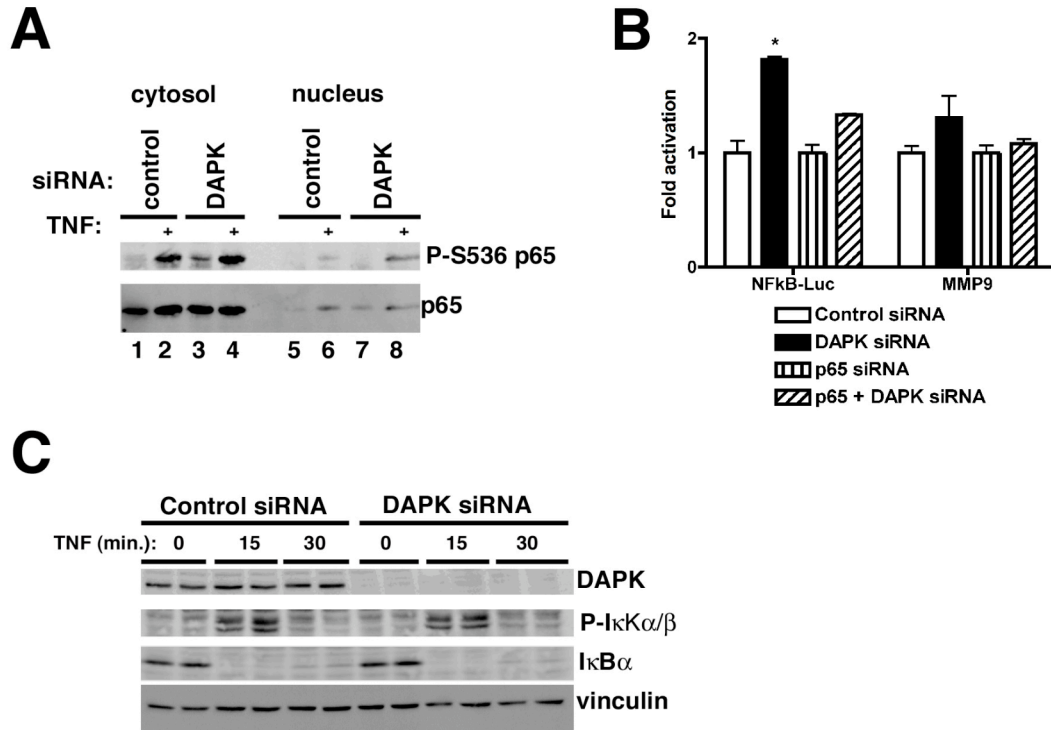
Figure 10: Increased MMP9 in DAPK-depleted HCASMC requires p65 phosphoS536.

A: HCASMC were Nucleofected with control or DAPK siRNA. Three days after Nucleofection, cells were serum-starved overnight. Cells were treated with or without TNFα (10 ng/ml) for 15 minutes to induce phosphorylation and nuclear translocation of p65. Cytosolic and nuclear fractions were prepared, and equal amounts were immunoblotted for p65 phosphoS536 and total p65. B: HCASMC were Nucleofected with siRNAs as indicated. Three days after Nucleofection, cells were Nucleofected again with NF-κB-Luc or wild-type MMP9 promoter construct and pTK-Renilla and the cells were plated in growth medium. After incubation for 18h, duplicate measurements were made for triplicate wells. The fold activation of promoter constructs was determined by normalizing to either control siRNA only, or to p65 siRNA only samples. *p<0.05 vs. control siRNA. C: Cells were treated as in A, except that RIPA lysates were prepared. Immunoblotting of TNFα (10 ng/ml) treated HCASMC revealed no difference in IκKα/β activation on S176/S180.

Table 1: Primers used for RTPCR

Primer name		Sequence (5' to 3')
Mo DAPK	Forward	ATG GCT ATT ACT CCG TGG CTA AAG
	Reverse	TCA CAG CAA GAT GAA GAG CGA TG
Mo RPLP0	Forward	GGA CCC GAG AAG ACC TCC TT
	Reverse	TGC TGC CGT TGT CAA ACA CC
Hu MMP9	Forward	GAA CCA ATC TCA CCG ACA GG
	Reverse	GCC ACC CGA GTG TAA CCA TA
Hu HPRT	Forward	CCT TGG TCA GGC AGT ATA ATC CA
	Reverse	GGT CCT TTT CAC CAG CAA GCT
Hu VCAM1	Forward	CAT GGA ATT CGA ACC CAA AC
	Reverse	TGT ATC TCT GGG GGC AAC AT

Chapter III: Generation and Characterization of a DAPK Knockout Mouse

Introduction

In the previous chapter, studies were described that addressed the role of DAPK in primary smooth muscle cells. This chapter outlines studies that address the role of DAPK *in vivo*. Much of the previous work regarding DAPK has been accomplished using cultured cell lines. A mouse model containing an in-frame deletion of part of the N-terminal kinase domain of DAPK has been generated and the resultant mouse expresses DAPK that lacks only a small region of the kinase domain (8, 63, 78). This animal is poorly characterized and its usefulness is limited by the fact that only a small region of the 160 kD DAPK protein is deleted to result in expression of nearly the entire molecule. Two other recent studies have been published which utilized two additional, independently generated DAPK knockout mouse models (42, 118). Gozuacik, et al. (2008) examined the effect of DAPK on ER stress in their DAPK knockout model, and found that DAPK is required for ER stress in kidney injected with thapsigargin. Tu et al. (2010) used a separate DAPK knockout mouse to examine the role of DAPK in a stroke model; they found that DAPK mediates neuronal death in response to stroke. Both of these models were generated using traditional, global gene knockout strategies. Up to this point, there have been no *in vivo* studies examining the effect of deletion of DAPK on vascular physiology and pathology. To accomplish this, a DAPK knockout (DAPK KO or DAPK$^{-/-}$) mouse model was generated.

Because of concerns that deletion of DAPK in all tissues could induce embryonic lethality, the choice was made to generate a conditional knockout mouse using the Cre-lox system. In addition, such a system offers many advantages over traditional knockout strategies, in that the control of deletion can be spatially and temporally regulated, depending on the Cre deleter mouse that is used. Thus, this chapter describes the first mouse containing a floxed DAPK gene. The generation and characterization of this mouse is outlined, together

with results from the carotid artery ligation injury model in which we sought to examine the effects of deletion of DAPK on the response to vascular injury *in vivo*. In this model, the right carotid artery is ligated, which prompts remodeling of the artery, increased MMP9 expression, and formation of a thickened medial smooth muscle layer and a neointimal layer in the lumen of the artery.

Methods

Generation of DAPK^{fl/fl} mice. The BAC Engineering Core at the University of North Carolina generated the targeting vector shown in **Figure 11**. The BAC clone used in its construction (RPCI-105I10) was originally isolated from C57BL/6. After sequencing to confirm the location of the elements listed in **Figure 11**, the Indiana University Transgenic Mouse Core Facility generated ES clones resistant to neomycin by electroporating the construct into albino C57BL/6 ES cells, and the resulting clones were grown and screened for homologous recombination of the floxed DAPK allele by PCR, Southern blotting, and sequencing of PCR-amplified floxed allele. ES clones were injected into C57BL/6 blastocysts, and the resulting chimeras were mated to wild-type C57BL/6 to check for germline transmission. DAPK^{fl/+} heterozygotes were obtained and confirmed by PCR analysis, and crossed with each other to generate DAPK^{fl/fl} homozygotes. The neo cassette was removed by mating the DAPK^{fl/fl} female with a male mouse expressing the FLPe recombinase under control of the β-actin promoter (Actin-FLPe^{+/+}; Jackson Laboratories).

Generation of DAPK-/- mice. To generate DAPK^{-/-} mice, male DAPK^{fl/fl} mice were mated with smMHC-Cre^{+/-} females. The smMHC-Cre+/- were obtained from Michael Kotlikoff (37, 125). Due to transient expression of Cre in these mice in eggs, this cross resulted in deletion of exon 4 in the floxed DAPK allele in the eggs, resulting in mice heterozygous for the DAPK allele in all tissues. The heterozygous smMHC-Cre^{+/-} DAPK^{+/-} females were then crossed with DAPK^{fl/fl} males to generate DAPK knockout (DAPK KO or DAPK^{-/-}) mice.

Southern blotting. Genomic DNA was isolated from ES cell clones, and 2-5 μg was digested with BamHI. The digests were separated on a 0.8% agarose gel, the gel was incubated in 0.25 M HCl followed by 0.4 M NaOH, and DNA was transferred to positively charged nylon filter (Brightstar Plus, Ambion), in 0.4 M NaOH by downward capillary transfer. A ^{32}P-labeled DNA probe was prepared using a agarose-gel purified, PCR-amplied fragment located 2140 nucleotides upstream of DAPK exon 4, following ^{32}P-labeled using the NEBlot kit (New England Biolabs). After neutralization in 2x SSPE, the membrane was incubated in hybridization buffer (6x SSPE, 5x Denhardt's solution, 0.5% SDS, and 100 μg/ml salmon sperm DNA) at 65°C for 3 hours. The ^{32}P-labeled probe was added and the blot was incubated at 65°C overnight with agitation. The membrane was washed and exposed to X-OMAT AR film (Kodak) with intensifying screens at -80°C. Expected sizes are 5.8 kb for wild-type allele and 4.5 kb for the recombined, floxed allele. BAC clones were used as controls; unmodified clone RPCI-105I10 was a wild-type control, and a modified BAC clone containing the neo cassette and loxP sites surrounding DAPK exon 4 was used as a control for the floxed, recombined allele. Both BAC clones were supplied by the BAC Engineering Core (UNC).

Genotyping. For screening of ES clones, genomic DNA was isolated from cells using the Gentra Puregene Cell Kit (Qiagen). For screening of mice, digits were cut from 12-14 day-old mouse pups. DNA was extracted by boiling the digits in 125 ml 25 mM NaOH and 0.2 mM EDTA for 30 minutes, followed by addition of 125 ml 40 mM Tris-HCl (117). PCR amplification was done using GoTaq Green Master Mix (Promega), 0.5mM each primer, and DNA. PCR method was: 95°C for 2 minutes, followed by 35 cycles of 95°C for 30 seconds, 55°C for 30 seconds, and 72°C for 1 minute. Amplicons were separated on a 1.4% agarose gel, and photographed using a Syngene GeneSnap. Primer sequences used for

genotyping are listed in **Table 2**. Sequencing of PCR amplicons to verify the distal loxP site was performed by Seqwright.

Real-time RT-PCR. Mouse tissues were rinsed in PBS and then snap-frozen in liquid nitrogen. RNA was prepared from frozen mouse tissues by homogenizing the tissue in Trizol (Invitrogen), using increased amounts of glycogen (200 μg per artery) to precipitate the small amount of RNA obtained from individual carotid artery samples. Tests were performed to verify that the increased glycogen present in the RNA samples did not interfere with subsequent cDNA production, nor PCR amplification. 0.5 μg of RNA was reverse transcribed as previously described (131). cDNA was diluted 1:5 with water, then amplified using Faststart SYBR green master mix (Roche) and gene specific primers (Eurofins MWG/Operon) in a AB 7500 Real-Time System (Applied Biosystems). Relative abundance of mRNA was calculated using the $2^{-\Delta\Delta Ct}$ method. HPRT was used as an internal control. Primer sequences used are listed in **Table 3**.

Semi-quantitative RT-PCR. RNA and cDNA was prepared as described above. DAPK exon 4 and HPRT were amplified using gene-specific primers (see Table 3). PCR was performed with the following cycling parameters: 95°C for 2', followed by 95°C for 30 seconds, 57°C for 30 seconds, and 72°C for 30 seconds for 30 cycles (HPRT) or 35 cycles (DAPK). Amplified DNA was separated on a 1.4% agarose gel, and photographed using a Syngene G-Box and GeneSnap software (Synoptics).

Immunoblotting. Tissues were homogenized in RIPA lysis buffer containing protease inhibitor cocktail and phosphatase inhibitor cocktails 1and 2 (Sigma), using a glass tissue homogenizer. Protein was quantitated using BCA assay (Pierce). Equal amounts of proteins were separated by SDS-PAGE, and detected using standard immunoblotting protocols. Antibodies used were: MMP9 (a generous gift of Dr. Robert Senior (Washington University, St. Louis, MO) (5);

46

DAPK (from BD Biosciences); GAPDH (Novus); vinculin, α-sm-actin, and β-actin from Sigma. Immunoblots were imaged using a Syngene G-box and GeneSnap software (Synoptics). Quantitation of band intensity was performed using ImageJ (NIH).

Gelatin zymography. Zymography was performed as previously described with a few revisions (73). Equivalent amounts of protein from RIPA lysates of tissues (20-50 μg) were separated by SDS-PAGE containing 7.5% acrylamide and 0.1% gelatin (Biorad). Gels were incubated in 2.5% Triton-X-100 for 30 minutes, then incubated in zymography buffer overnight at 37°C. (50 mM Tris pH 7.5, 200 mM NaCl, and 5 mM $CaCl_2$). Gels were stained in 0.5% Coomassie Blue R-250 in 7.5% methanol/7.5% acetic acid for 24 hours, followed by destaining in 7.5% methanol/7.5% acetic acid for 2 hours. Gels were dried and photographed using a Syngene G-box and GeneSnap software (Synoptics).

Carotid artery injury model. Eight-week old DAPK^{fl/fl} or DAPK^{fl/+} and DAPK-/- mice underwent the carotid ligation surgery as previously described with a few modifications (69). Briefly, mice were anesthetized with a cocktail of ketamine (0.1 mg/g) and xylazine (0.01 mg/g). The carotid artery was exposed via a 0.5-cm incision 1-mm from the midline on the mouse's neck. A 4-0 silk suture was used to ligate the right common carotid artery, proximal to the bifurcation. For RNA and protein analysis, mice were sacrificed 1-14 days following injury, and the injured carotid artery rinsed in PBS and frozen in liquid nitrogen. Uninjured carotid arteries from mice that did not undergo surgery were used as controls. Lysates were prepared by grinding the frozen arteries in RIPA buffer containing protease and phosphatase inhibitors (Sigma) using a glass tissue homogenizer. For histological analysis, injured mice were anesthetized and then perfused, first with sterile saline (0.9%) containing 0.1 mM sodium nitroprusside and 1 mM adenosine, and then with RNAlater (Ambion). Arteries were fixed overnight in Z-Fix (Anatech) and embedded in paraffin. Sections obtained 50 μm from the

suture were stained with Verhoeff-van Gieson elastin stain. Embedding, sectioning, and staining was performed by the Indiana University Anatomy and Cell Biology Histology Core. Images were obtained from a Nikon Eclipse 90i microscope, Nikon DS-Fil camera and Nikon Elements AR 3.0 software. Images were compiled in Adobe Photoshop. ImageJ was used to measure intima and neointimal areas in injured arteries. The intima was defined as the area between the inner and outer elastic lamina, and the neointima was defined as the area of cells and connective tissue (not blood cells) on the inside of the inner elastic lamina. At least two sections were measured for each artery and the average area was used in statistical analyses.

Animal studies. All animal studies were approved by Indiana University IACUC.

Data analysis. All experiments were independently performed at least three times. All statistical analysis and graphs were created using GraphPad Prism software (GraphPad Software, San Diego, CA). Graphs display mean +/- sem of at least three independent experiments. Statistical significance was determined by Student's t test unless otherwise noted.

Results

In order to determine the *in vivo* role that DAPK plays in mouse physiology, we sought to generate a DAPK knockout mouse. Previous data from this and other laboratories using cultured cell systems indicated a role for DAPK in regulating apoptosis and autophagy (8, 78). In light of this, and in order to allow the greatest flexibility in deleting DAPK from specific tissues, a DAPK flox/flox (DAPK$^{fl/fl}$) mouse was generated, such that loxP sites flanked exon 4. These loxP sites can be acted upon by Cre recombinase to generate either a whole-body or a tissue specific deletion of DAPK. **Figure 11** shows the targeting strategy used to generate the DAPK$^{fl/fl}$ mouse. Following Cre recombinase activity, exon 4 will be deleted. Deletion of exon 4 is expected to result in splicing

of exon 3 to exon 5 to generate a frame shift that incorporates a translational stop codon after 3 missense amino acid residues. The subsequent mRNA will encode a protein comprised of the first 95 amino acids together with 3 miscoded amino acids. This region of DAPK contains 81 residues of the kinase domain but will not be functional as all of the known conserved kinase domain motifs are deleted (44). The targeting construct encodes the gene for neomycin, which is used for positive selection, as well as a negative selection cassette encoding diptheria toxin. The targeting construct was linearized and electroporated into albino C57BL/6 ES cells (Stratagene), and resulting clones were screened by PCR. The PCR primers were positioned (**Figure 12A, P1/P6)** such that they would allow identification of correct targeting of the neo/flox cassette following electrophoresis of the PCR reaction products. Representative results are shown in **Figure 12C**; a 1.2-kb band was detected in the amplified DNA from the DAPK$^{fl/+}$ mice with primers P1/P6. In addition, Southern blotting was performed to verify clones with correct targeting of the neo/flox cassette following hybridization with an appropriate probe (**Figure 12A). Figure 12B** shows the result of the Southern blot experiments. As expected, the ^{32}P-labeled probe hybridized with a 5.8-kb BamHI-fragment in DNA samples from negative control, non-electroporated ES cells, consistent with the expected results based on the sequence of the wild-type DAPK allele. A 5.8-kb wild-type band and a 4.5-kb band that corresponds to the size expected by the recombined allele hybridized to the labeled probe in DNA samples from heterozygous, DAPK$^{fl/+}$ ES cells. BAC DNA was used as positive and negative controls for the Southern blot. Because of difficulties in finding unique restriction sites in the right targeting arm 3' of exon 4, Southern blotting used to verify the correct placement of the distal loxP site between exon 4 and 5 was inconclusive. To validate the correct placement of the distal loxP site, this region was amplified by PCR using primers P2 and P5, and then sequenced to verify the correct placement of both loxP sites. Two independent ES clones (#244 and #315) containing correctly-targeted, floxed-exon 4 were injected into C57BL/6 blastocysts, and implanted into pseudopregnant females to generate

49

two independent DAPK$^{fl/+}$ lines. The resulting chimeric pups were then mated with wild-type C57BL/6 mice, and the pups were screened by PCR with primers P2 and P5, as is shown in **Figure 12A and D**.

In order to delete the neomycin cassette, female DAPK$^{fl/+}$ mice were mated with a male, C57BL/6 ACTFLPe mouse expressing the FLP recombinase under the control of the human ACTB promoter. This mating resulted in recombination between the FRT sites flanking the neomycin cassette and deletion (Δneo) of this cassette (**Figure 11**). The resulting DAPK flΔneo/+ mice (Figure 13A) were then backcrossed to each other to generate homozygous DAPK$^{floxΔneo/floxΔneo}$. The genotype of this strain was verified by PCR, using primers P1 and P4 as shown in **Figure 13A**. The PCR resulted in generating a single 0.7-kB fragment corresponding to a DAPK$^{floxΔneo/floxΔneo}$ mouse; DAPK$^{floxΔneo/+}$ mice generated both a 0.7 kb fragment, and a 0.6kb wild-type fragment (**Figure 13A**).

To generate a full-body DAPK$^{-/-}$ mouse, a DAPK$^{floxΔneo/floxΔneo}$ male was mated with a C57BL/6 smMHC-Cre$^{+/-}$ female. This smMHC-Cre mouse expresses Cre recombinase under control of the smMHC promoter. Due to a transient expression of Cre in the egg, in which the Cre protein is present in both Cre genetically positive and negative fertilized eggs, crossing a male DAPK$^{floxΔneo/floxΔneo}$ with a female Cre$^{+/-}$ mouse results in all progeny having one DAPK allele deleted (DAPK$^{+/-}$). Crossing the heterozygous DAPK$^{+/-}$ mice generated a full-body DAPK$^{-/-}$ line. The PCR results are shown in **Figure 13B**, confirming deletion of the DAPK exon 4 (primers P3 and P4, 0.35-kB fragment), and the presence of the recombined DE4 allele (primers P1 and P5, 0.72-kB fragment).

The deletion of DAPK exon 4 was confirmed by RT-PCR of RNA isolated from liver, using primers that spanned exons 3 and 4 to generate the expected 0.2-kB fragment (**Figure 14A)**. Primers to HPRT, which generated a 0.2-kB fragment, were used as a positive control to confirm the presence of RNA in all samples. In addition, the absence of DAPK protein was confirmed by immunoblotting lysates prepared from liver and brain tissues from DAPK$^{+/+}$,

DAPK$^{-/-}$, and DAPK$^{+/-}$ mice. These tissues were selected because they have high levels of DAPK expression. As is shown in **Figure 14B**, no DAPK protein was found in the liver or brain of DAPK$^{-/-}$ mice, and as expected reduced levels were observed in DAPK$^{+/-}$ mice.

Examination of the DAPK$^{-/-}$ mice yielded no overt visible differences caused by the deletion of the DAPK protein. The DAPK$^{-/-}$ mice exhibited no changes in weight, when compared with wild-type counterparts from the same colony (**Figure 15A**). A reduction the sizes of litters from DAPK$^{-/-}$ mice was observed; **Figure 15B** shows that both DAPK$^{-/-}$ lines 244 and 315 exhibited reduced litter sizes, possibly indicating that there may be some reproductive problems or issues with the survival of some DAPK KO pups. The frequency of genotypes resulting from DAPK heterozygote crosses (DAPK$^{+/-}$ x DAPK$^{+/-}$;from line 244), and from DAPK$^{-/-}$ and DAPK$^{+/-}$ (line 315) are shown in **Table 4**. For line 244, there was a reduction in the expected percentage of DAPK$^{-/-}$ resulting from heterozygous parents (21% vs. the expected 25%); the reduction was more striking with males (13%). In addition, a reduction in the number of DAPK$^{-/-}$ was observed in line 315 (44% vs. the expected 50%). A Chi-squared analysis did not show that the difference is statistically significant and it is likely due to the small sample size for this study. It should be noted that this result agrees with a previous study that showed that male DAPK$^{-/-}$ mice were born at lower than expected frequencies (42). In the current study, two DAPK$^{fl/fl}$ and DAPK$^{-/-}$ lines were maintained (lines 244 and 315), and no differences have been observed between the lines. Data presented are from line 244, unless otherwise noted.

Data presented in **Chapter II** pointed to a role for DAPK in regulating MMP9 expression in vascular smooth muscle, with increased MMP9 mRNA and protein measured from HCASMC that had been depleted of DAPK using a DAPK siRNA. In order to determine if *in vivo* deletion of DAPK results in altered MMP9, immunoblotting and zymography was performed on RIPA lysates from mouse aorta obtained from DAPK$^{fl/fl}$ and DAPK$^{-/-}$ mice. Low levels of MMP9 protein were observed in the aorta; however they were not different between DAPK$^{fl/fl}$ and

51

DAPK$^{-/-}$ mice. (**Figure 16A**). The expression of MMP9 protein was lower in other tissues, such as carotid artery, liver and kidney, so qRT-PCR was used to detect changes in MMP9 mRNA. As is shown in **Figure 16B**, there was no change in the levels of MMP9 mRNA in carotid artery, liver or kidney tissues obtained from DAPK$^{-/-}$, as compared with the same tissues obtained from DAPK$^{fl/fl}$ mice.

This result was surprising, especially in the aortic vascular tissue, as we had previously found that DAPK was a negative regulator of MMP9 in cultures of primary HCASMC (**Chapter II**, **Figure 3**). One possible explanation for this result is that in DAPK$^{-/-}$ mice a compensatory mechanism is engaged which blocks increased MMP9 expression. This possibility is not implausible, as increases in this protease are likely undesirable and incompatible with normal physiology. In support of this, macrophage specific transgenes overexpressing this protease have been described as having adverse effects on recruitment of neutrophils based on MMP9 activity inactivating certain chemokines (14, 119). However, compensation in whole animal knockouts is often not able to rescue the effects of the knockout under pathological conditions. In order to determine if DAPK has effects on MMP9 expression in an *in vivo* pathological condition, we examined the response of DAPK$^{-/-}$ mice to carotid artery ligation. This injury, which is schematically illustrated in **Figure 17A**, mimics blockage of arteries by thrombus formation, and results in the remodeling of the ligated artery (69). This remodeling is characterized by migration and subsequent proliferation of the medial smooth muscle cells in the lumen of the artery. Within 24h after ligation, a significant increase in MMP9 expression has been observed (40), indicating that this model would be appropriate to test the hypothesis that DAPK negatively regulates MMP9 *in vivo*. **Figure 17B** shows the results from western blotting of lysates prepared from the injured carotid arteries of a DAPK$^{+/+}$ mouse. These results established the time course of expression of MMP9 and showed that in response to carotid ligation, the levels of MMP9 in the injured vessels increased from undetectable basal levels until 4 days post-injury, after which time the levels of MMP9 began to decrease and continued to do so until at least 14 days after

injury. In addition, this experiment verified previous observations that expression of smooth muscle markers, such as smooth muscle α-actin (sm-α-actin) decreased over the first 7 days post-injury. This is likely due to de-differentiation of the vascular smooth muscle from contractile cells to more proliferative, migratory cells in response to the injury. In parallel, there was an increase in DAPK protein was observed as early as 4 days after injury, and maintained until at least 14 days post-injury (for quantification, see **Chapter II, Figure 3C**). Since both DAPK$^{fl/fl}$ and DAPK$^{fl/+}$ were used as controls in this study the control mice will be denoted as DAPK^{fl}. **Figure 18A** and **Figure 18B** shows the results of western blots and gelatin zymograms of uninjured and injured carotid arteries at 1 and 7 days post-injury. Quantification of these results revealed that there was a 9.6-fold increase in MMP9 levels within 1 day following injury in DAPK^{fl} mice.

Based on the findings in cultured primary HCASMC (**Chapter II**), we expect DAPK to negatively regulate MMP9 expression. Thus, the DAPK$^{-/-}$ mice should exhibit an increase in MMP9 expression in injured carotid arteries, compared to DAPK^{fl} mice. Unexpectedly, MMP9 levels at 7 days post-injury were actually lower in DAPK$^{-/-}$ mice compared to DAPK^{fl} mice (**Figure 18B**). To quantify the levels of active MMP9 expressed in response to the ligation injury the intensity of MMP9 bands (**Figure 18C**) was quantitated and normalized to vinculin, which was used as a loading control. As is shown in **Figure 18C** there was no difference in expression of MMP9 observed at 1 day post-ligation, and although the effect at 7 days is not statistically significant, the trend indicates that DAPK$^{-/-}$ have lower levels of MMP9. To further verify these unexpected results, qRT-PCR was performed to measure MMP9 mRNA in injured and uninjured carotid arteries from control DAPK^{fl} and DAPK$^{-/-}$ mice. As **Figure 18D** shows, ligation injury of the carotid artery resulted in a 12.5-fold increase in MMP9 mRNA, and there was no difference between DAPK^{fl} and DAPK$^{-/-}$ mice (12.5 +/- 3.0 for DAPK^{fl} vs. 14.1 +/- 2.3 for DAPK$^{-/-}$).

Histological sections of carotid artery tissues were prepared from DAPK^{fl} and DAPK$^{-/-}$ mice at 14 (**Figure 19 A-D**) and 28 days (**Figure 19 E-H**) post-

ligation injury. These sections were stained with Verhoeff-van Giesen stain to visualize morphological details of the tissues including the adventitial, medial and neointimal layers as well as the elastic laminae. Representative stained sections were examined at these two time points and this examination revealed an increase in the thickness of the medial smooth muscle in response to the carotid ligation injury (**Figure 19**). As can be seen by comparing panels A, B to C, D of **Figure 19**, DAPK$^{-/-}$ mice had reduced response to injury at 14 days. For comparison an uninjured control DAPK^{fl} artery is shown in **Figure 19-I** Quantitation of the medial smooth muscle areas in these sections revealed that DAPK$^{-/-}$ mice had significantly smaller medial smooth muscle areas at 14 days after injury (**Figure 19 A-D, and 19J**). This trend was not observed at 28 days post-injury, however (**Figure 19 E-H and 19J**).

DAPK has been previously implicated as a negative regulator of fibroblast and cancer cell migration(71). Results presented in **Chapter II (Figure 2)** indicated that DAPK also negatively regulates smooth muscle cell migation. Because the carotid ligation injury results in migration of smooth muscle cells into the lumen of the vessel to form a neointima, we hypothesized that the DAPK$^{-/-}$ mice would exhibit increased SMC migration in response to injury, resulting in an increased neointimal area at later time points post injury. The response to injury at 14 and 28 days post-injury in both the DAPK^{fl} mice and DAPK$^{-/-}$ was quite varied; as is shown in **Figure 19E-H**, and many but not all mice showed development of a neointima at these time points. The ratio of neointimal to medial smooth muscle area is commonly used to compare the response to injury in vascular models. The quantitative results shown in **Figure 19K** reveal the heterogeneity in the response at 28 days, and suggest that there is no significant difference between the medial area or the neointimal/media ration for DAPK^{fl} and DAPK$^{-/-}$ mice. Interestingly, on average, the DAPK$^{-/-}$ mice do show a trend toward having decreased neointimal formation at 14d post-injury (**Figure 19K**), with means of 0.203 +/- 0.08 in the DAPK$^{fl/fl}$ and 0.079 +/- 0.04 for the DAPK$^{-/-}$.

Discussion

The data presented in this chapter are the results of studies following the generation of a DAPK knockout mouse. These studies show that we successfully generated a transgenic mouse containing loxP sites flanking exon 4 of DAPK. A heterozygous mouse was then generated by mating a male DAPK$^{fl/fl}$ mouse with a mouse that expresses Cre recombinase in eggs at the time of fertilization. Deletion of exon 4 was determined by PCR, RT-PCR, Southern, and immunoblotting. Analysis of mouse litter size indicated that the DAPK$^{-/-}$ mice produce significantly smaller litters than DAPK$^{+/+}$ mice. In addition, when the numbers of DAPK$^{-/-}$ mice generated from heterozygous crosses were tabulated, there was a trend toward a decrease in the birth of DAPK$^{-/-}$ pups. Although the trend was not statistically significant due to the small sample size, it is likely that deletion of DAPK presents a challenge to the survival of mice during embryonic development.

Based on the results from **Chapter II** showing that DAPK is a negative regulator of MMP9 in human coronary artery smooth muscle cells, it was hypothesized that deletion of DAPK would result in increased MMP9 expression. However, no changes were observed in MMP9 mRNA or protein levels in several tissues, including aorta, carotid artery, liver, and kidney, although future work should include more samples, to verify the results in liver and kidney, and to allow for statistical analysis of the data. Using the carotid artery ligation injury model, the effect of DAPK deletion on MMP9 levels in a pathological condition was tested. Both DAPK$^{-/-}$ and DAPK^{fl} mice displayed a similar, robust increase in MMP9 protein and mRNA 1 day after injury. The MMP9 levels remained increased about basal up to 14 days following injury. Interestingly, in the DAPK$^{-/-}$ mice, there was a trend toward a reduction in the MMP9 protein observed 7d after injury, although future studies should first expand the sample size to allow statistical analysis of the quantification. In addition to inducing MMP9 expression, the carotid artery ligation also causes smooth muscle cell migration and proliferation to result in a thickened medial smooth muscle layer and the

generation of a neointimal cell layer that encroaches upon the lumen of the vessel. Examination of histological sections from DAPK^{fl} and DAPK$^{-/-}$ mice showed no significant difference in neointimal formation, however DAPK$^{-/-}$ mice generate significantly smaller medial smooth muscle layers 14 days following injury.

The results in this study were surprising in many ways, but are instrumental in leading us to new areas in which to determine the *in vivo* role of DAPK. Based on the studies in **Chapter II** and previous studies, it was expected that DAPK$^{-/-}$ mice might have a myriad of problems which would be detrimental to their development. The strategy of using the Cre-lox system was decided upon because it was thought that deletion of DAPK in all tissues might induce embryonic lethality. During the generation of these mice, studies were published using adult mice from two independently-generated DAPK$^{-/-}$ mouse models (42, 118). These studies indicated that our DAPK$^{-/-}$ mice would not likely be embryonic lethal. The DAPK$^{-/-}$ mice in our study exhibited normal growth, compared to the DAPK$^{fl/fl}$ mice that have normal levels of DAPK. Based on the results in Table 4, there was a trend toward reduced numbers of the DAPK$^{-/-}$ mice born, especially with male mice. This is in agreement with a previous study, which found slight decreases in numbers of male DAPK$^{-/-}$ mice, when compared to expected Mendelian ratios (42). This observation indicates that DAPK has an important role in promoting the development and survival of mice *in utero*. This also lends credence to the hypothesis that the surviving mice likely have alterations that allow them to compensate for the deleterious effects resulting from the loss of DAPK expression.

We observed increased MMP9 expression in HCASMC when DAPK was depleted in studies reported in **Chapter II**. In cell culture, these effects did not adversely affect cell survival, but in an *in vivo* system such as the DAPK$^{-/-}$ mouse, such increases would likely alter development and might not be compatible with life. MMP9 is a protease that can digest extracellular matrix proteins and growth factors, altering their activity (86, 87). Expression of MMP9 is tightly regulated by

many cytokines, and the activity is tightly regulated *in vivo* by the expression of endogenous inhibitors such as TIMP-3 (87). Previous studies have linked alterations in the balance of TIMPs and MMPs with vascular pathology, like aneurysm (3, 35, 66). In addition, transgenic mice constitutively expressing MMP9 in macrophages exhibited less stable atherosclerotic plaques on an ApoE$^{-/-}$ mouse background (41). An upregulation in MMP9 would likely be undesirable; thus the DAPK$^{-/-}$ mice that are born and survive likely have slight changes to reduce the expression.

Another reason for the different results observed in **Chapter II** versus this chapter is that the studies in **Chapter II** were performed in human coronary artery smooth muscle cells, and in this *in vivo* study was performed on vascular tissue from aorta and carotid arteries. It is possible that the effect might be a species difference or a tissue origin difference, or that the signaling pathways activated in SMC culture differ from those activated in the response to carotid injury. The carotid injury model involves a more complex situation, with multiple cells contributing to MMP9 expression.

Examination of the histological sections showed that DAPK$^{-/-}$ mice have smaller areas of medial smooth muscle. The decrease in MMP9 observed at 7d after injury could be contributing to the decreased medial smooth muscle area; however, more samples are needed to confirm the decrease in MMP9. Alternatively, the unexpected decrease in medial smooth muscle could be a direct effect of DAPK; previous work by this lab has found that primary aortic SMC require DAPK for survival (61). Perhaps the pathological conditions stimulated by the carotid injury result in apoptosis in SMC lacking DAPK.

In conclusion, DAPK$^{-/-}$ mice have been generated which display defects in the response to carotid injury. The DAPK$^{-/-}$ mice exhibit reduced MMP9 expression 7 days after injury. In addition, there is a decrease in medial smooth muscle area 14 days following injury. In **Chapter IV**, conclusions for these experiments are described and future studies are outlined to determine if there is a change in cell number, apoptosis, or proliferation. Studies will also seek to

identify the reason that DAPK has different effects on MMP9 expression in human CASMC and in the *in vivo* carotid injury model.
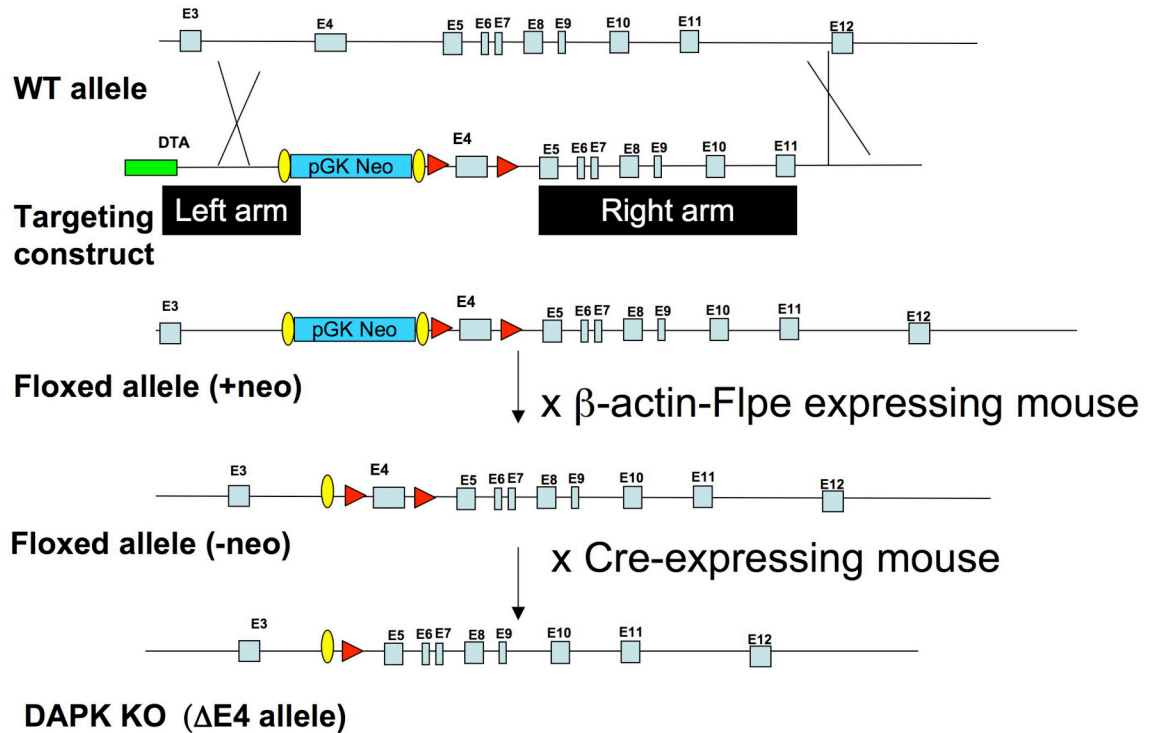
Figure 11: Strategy for generating DAPK^{fl} and DAPK$^{-/-}$.

A targeting construct was generated containing loxP sites flanking exon 4 of the DAPK1 gene (red triangles). A neomycin resistance cassette (pGK Neo) flanked by FRT sites (yellow ovals) and a diptheria toxin A (DTA) gene (green box) were included in the targeting construct for use as a positive and negative selection of ES cell transgenes. Homologous recombination between the targeting vector and the gene results in generation of the floxed allele (+neo). Subsequent mating with the Actin-FLPe mouse (FLPe recombinase under the control of the human β-actin promoter) results in floxed allele (Δneo). Deletion of exon 4 is accomplished by mating the floxed allele (Δneo) mouse with a mouse expressing Cre recombinase to generate ΔE4 allele. This study used smMHC-Cre deleter mice, which contain Cre in the fertilized egg, generating a whole-body deletion of the DAPK Exon 4 (ΔE4).
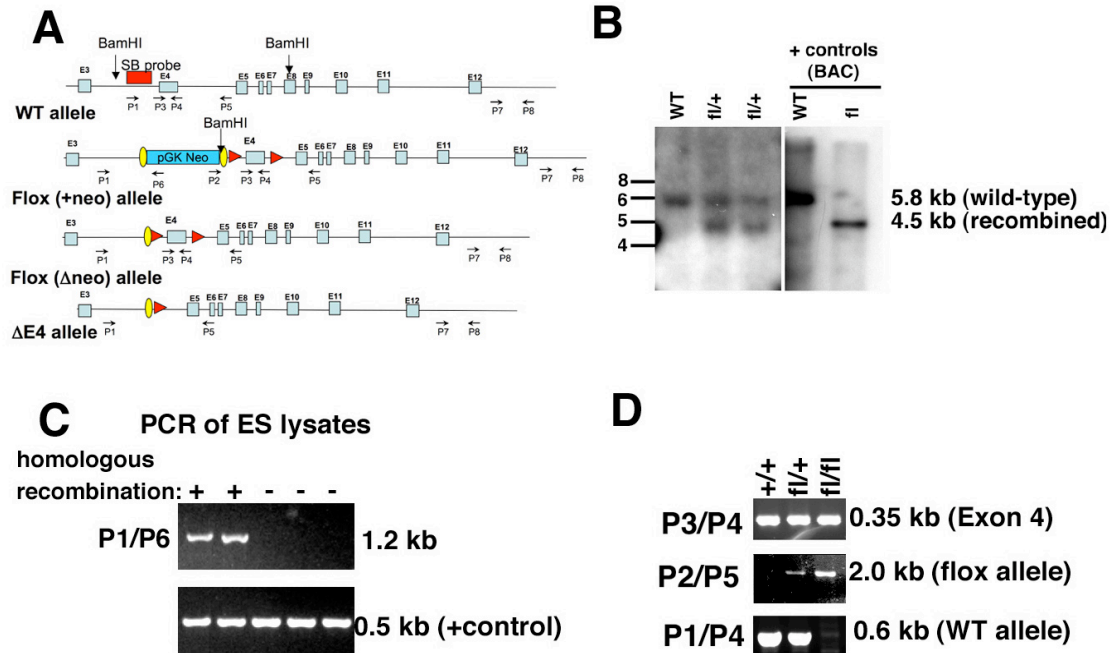
Figure 12: Verification of DAPK ^{fl}, DAPK $^{fl\Delta neo}$, and DAPK$^{-/-}$ mice.

A: Location of the primers used for PCR verification of the floxed DAPK and DAPK KO mice (P1-P8). In addition, the Southern blot probe (SB probe) location is shown (red box). B: Autoradiogram of a Southern blot showing the presence of the recombined, floxed DAPK allele (4.5-kb band) in two ES cell lysates, in addition to the wild-type DAPK allele (5.8 kb). BamHI was used to digest the genomic DNA, and the sites are indicated in panel A. Positive controls include BamHI digested BAC DNA (RPCI-105I10), which contains the section of the wild-type (WT) DAPK1 gene shown in panel A. The targeting construct shown in Figure 11 was homologously recombined with the WT BAC to generate the "fl" positive control shown on the right. C - D are representative images of agarose gels used to identify PCR reaction products. The primers used and the size of the expected fragment, are indicated on to the left and right sides of the gels, respectively. C: PCR results from ES cells to validate the occurrence of homologous recombination between DAPK exon 3 and exon 4. P1/P6 generated a 1.2 kb product in ES cells where homologous recombination occurred; no band was observed where random integration of the construct occurred. D: PCR

60

fragments generated from genomic DNA samples of the indicated genotypes of flox mice. The sizes of the fragments verify the presence of the DAPK^{fl/+} and DAPK^{fl/fl} alleles. P2/P5 primers amplify only the flox allele to generate a 2.0 kb fragment, P1/P4 primers will amplify only the WT allele to generated a 0.6 kb fragment and P3/P4 primers amplify within exon 4 to generate a 0.35 kb fragment.
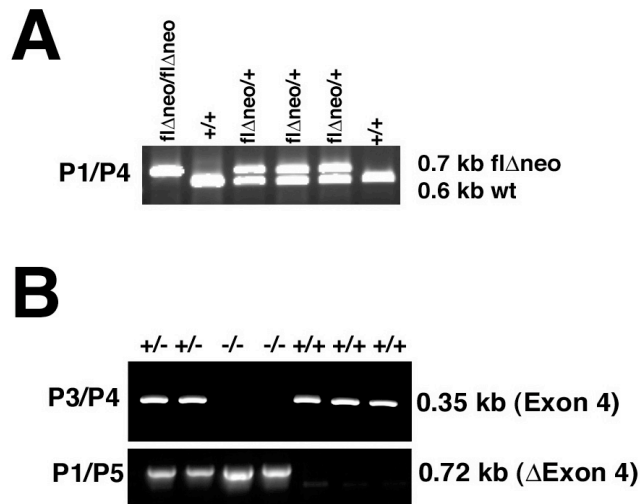
Figure 13: Verification of DAPK $^{fl\Delta neo/fl\Delta neo}$ **and DAPK** $^{-/-}$ **mice.**

A: PCR results from flox∆neo mice verify the presence of DAPK$^{fl\Delta neo/+}$ and DAPK$^{fl\Delta neo/fl\Delta neo}$ alleles. P1/P4 primers amplify a 0.7 kb region corresponding to the fl∆neo allele, and a 0.6 kb region corresponding to the wild-type (wt) allele. B: PCR results to verify the alleles of the DAPK$^{+/-}$ and DAPK$^{-/-}$ mice. P3/P4 primers amplify exon 4 to generate 0.35 kb amplicons for wild-type or the floxed allele but do not amplify the deleted exon 4 (∆Exon 4). P1/P5 primers generate a 0.72 kb amplicon for the ∆Exon 4 allele.
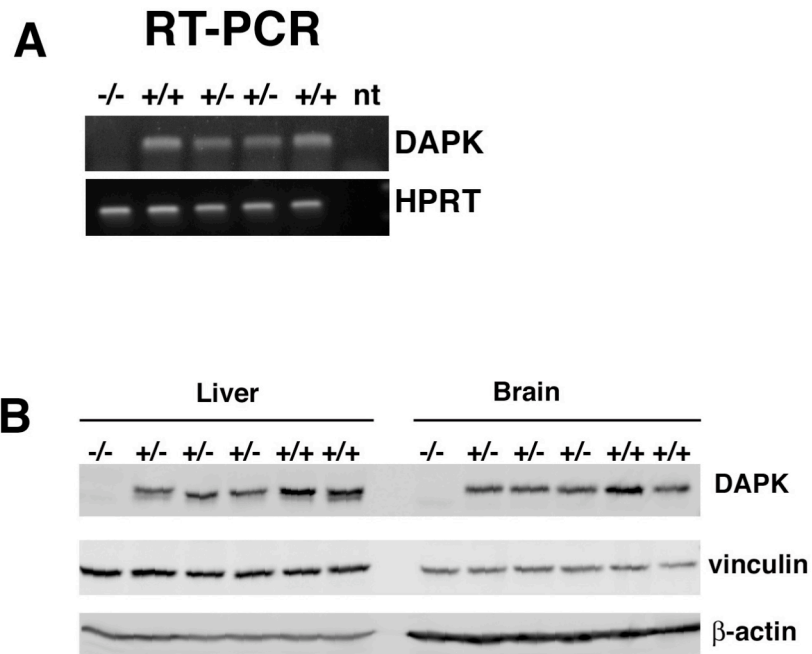
Figure 14: Verification of deletion of DAPK mRNA and protein.

A: Semi-quantitative RT-PCR was performed on liver RNA obtained from DAPK$^{+/+}$, DAPK $^{+/-}$, and DAPK$^{-/-}$ mice. DAPK$^{-/-}$ mice showed no amplification of the DAPK exons 3/4 (upper, lane 1) and DAPK$^{+/-}$ showed reduced levels when compared to DAPK$^{+/+}$. Primers to HPRT were used as an internal control. A no-template (nt) control was also tested. B: Immunoblotting verified the absence of DAPK protein in lysates from the liver and brain of DAPK KO mice, and reduced levels in lysates from DAPK$^{+/-}$. Anti-DAPK monoclonal antibody (Sigma) was used to detect expression of DAPK in 80 μg liver and 70 μg of brain cell extracts. Vinculin and β-actin were used as loading controls.
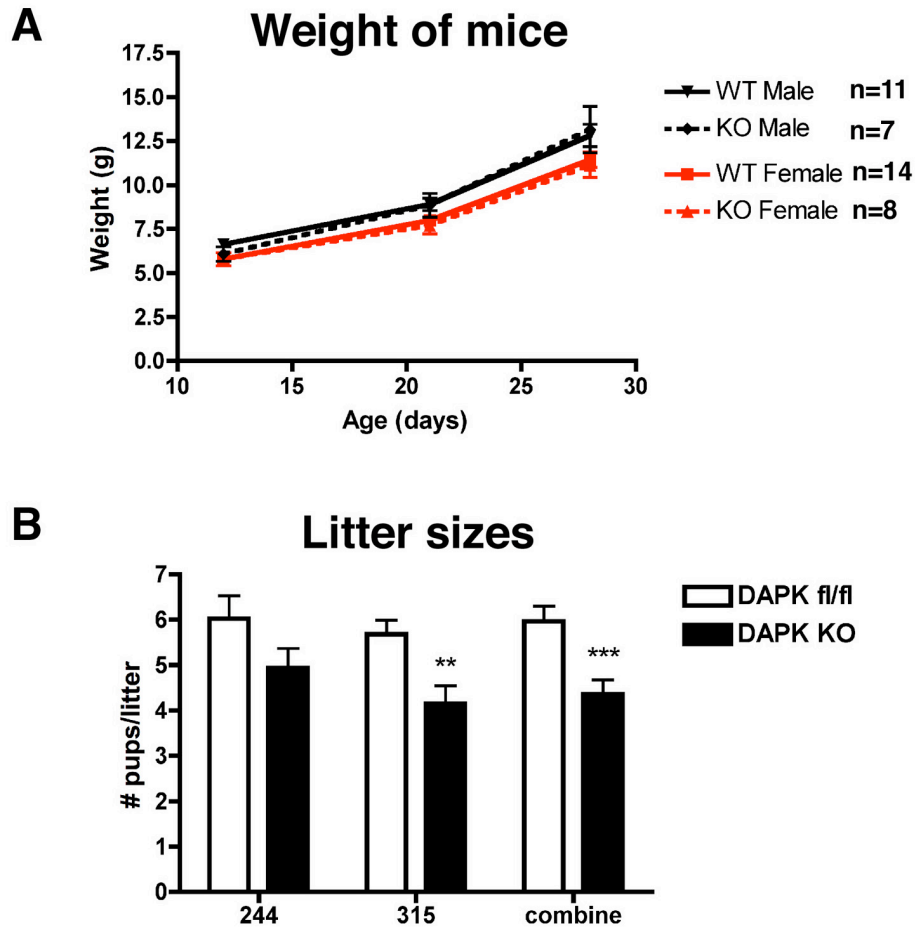
Figure 15: Statistical analysis of growth and litter size in WT and DAPK KO mice.

A: Weights of mice were tabulated at various times and graphed as indicated. WT litters were used for comparison because there were not enough DAPK^{fl/fl} litters at time of publication. B: Mouse litter sizes for two lines of DAPK^{fl/fl} or DAPK^{-/-} mice were tabulated and graphed as indicated. For the combined column, data from the 244 and 315 lines were combined. ** p<0.01, *** p<0.001. DAPK KO denotes DAPK^{-/-} genotype. Sample sizes were: 244 DAPK^{fl/fl} (n=34), 244 DAPK KO (n=29), 315 DAPK^{fl/fl} (n=25), 315 DAPK KO (n=21), combined DAPK^{fl/fl} (n=59), and combined DAPK KO (n=50).
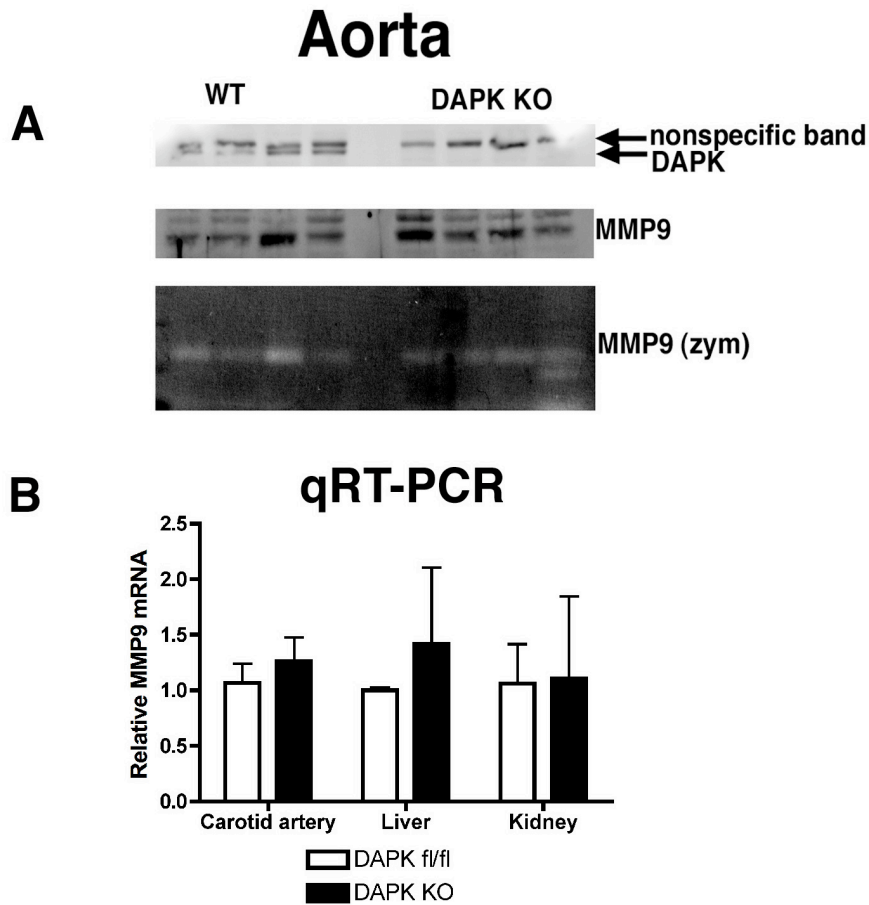
Figure 16: Quantitation of MMP9 protein and mRNA in DAPK$^{-/-}$ mice.

A: RIPA lysates from DAPK$^{fl/fl}$ and DAPK$^{-/-}$ (denoted DAPK KO) mice were analyzed by immunoblotting for DAPK (Sigma) and MMP9, and gelatin zymography. Each lane on the gel represents 50 μg total protein. B: qRT-PCR was performed on cDNA generated from total RNA prepared from carotid artery, liver, and kidney of control DAPK$^{fl/fl}$ and DAPK KO (DAPK$^{-/-}$) mice as indicated. MMP9 mRNA was normalized to HPRT. Values were then normalized to the average of the DAPK$^{fl/fl}$ group for comparison. N=6 for carotid artery, n=2 for liver and kidney.
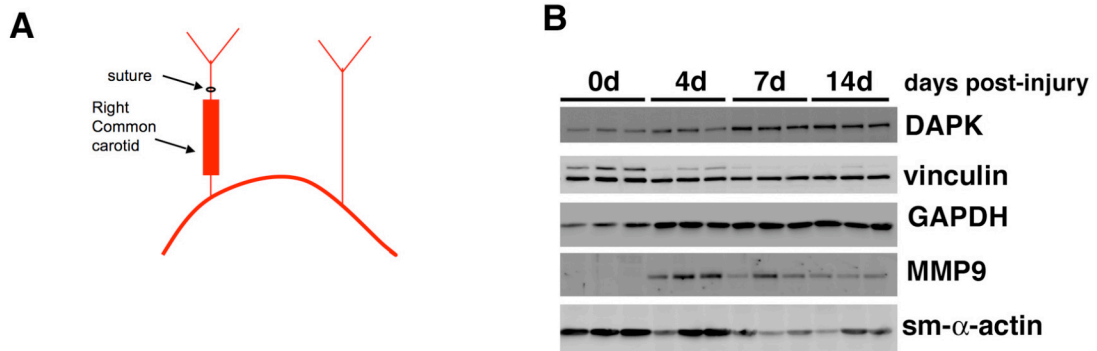
Figure 17: Expression of MMP9 is upregulated by carotid ligation.

A: Schematic showing the region of the right carotid artery ligated; the region highlighted by the box was collected for protein and mRNA analysis. B: Lysates from carotid arteries of WT C57BL/6 0-14 days post injury were analyzed as indicated. Immunoblotting results from mice showing the response to injury at the protein level from 0-14 days after injury. DAPK antibody was from BD. Carotid arteries from uninjured mice were used as negative controls. RIPA lysates (20 μg per lane) were blotted for the indicated proteins.
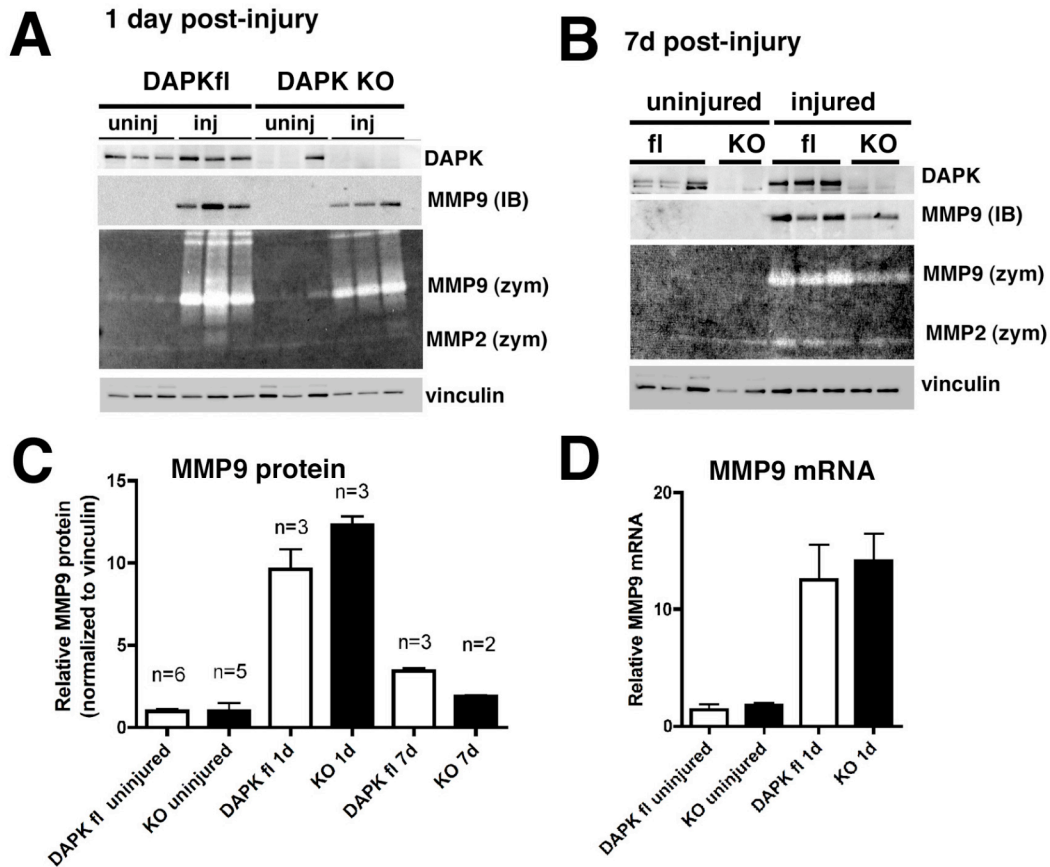
Figure 18: MMP9 is upregulated in both DAPK[fl] and DAPK [-/-] mice; MMP9 mRNA is decreased in DAPK^{-/-} mice at 7d after injury.

A-B: Lysates from carotid arteries of WT C57BL/6 1 and 7 days post injury were analyzed as indicated. Immunoblotting results from mice showing the response to injury at the protein level from 0-14 days after injury. Carotid arteries from uninjured mice were used as negative controls. RIPA lysates (20 μg per lane) were blotted for the indicated proteins. Immunoblotting and zymography results 1 day (A) and 7 days (B) post-injury from DAPK [fl] and DAPK^{-/-} mice (denoted DAPK KO). DAPK monoclonal antibody was from BD. C: MMP9 was quantitated on zymograms in A & B, and normalized to the immunoblotted vinculin. N values are as indicated. D: qRT-PCR was used to measure MMP9 mRNA in RNA

samples obtained from DAPK $^{fl/}$ or DAPK KO mice at 1 day post-injury. Levels were normalized to mouse HPRT. N=6.
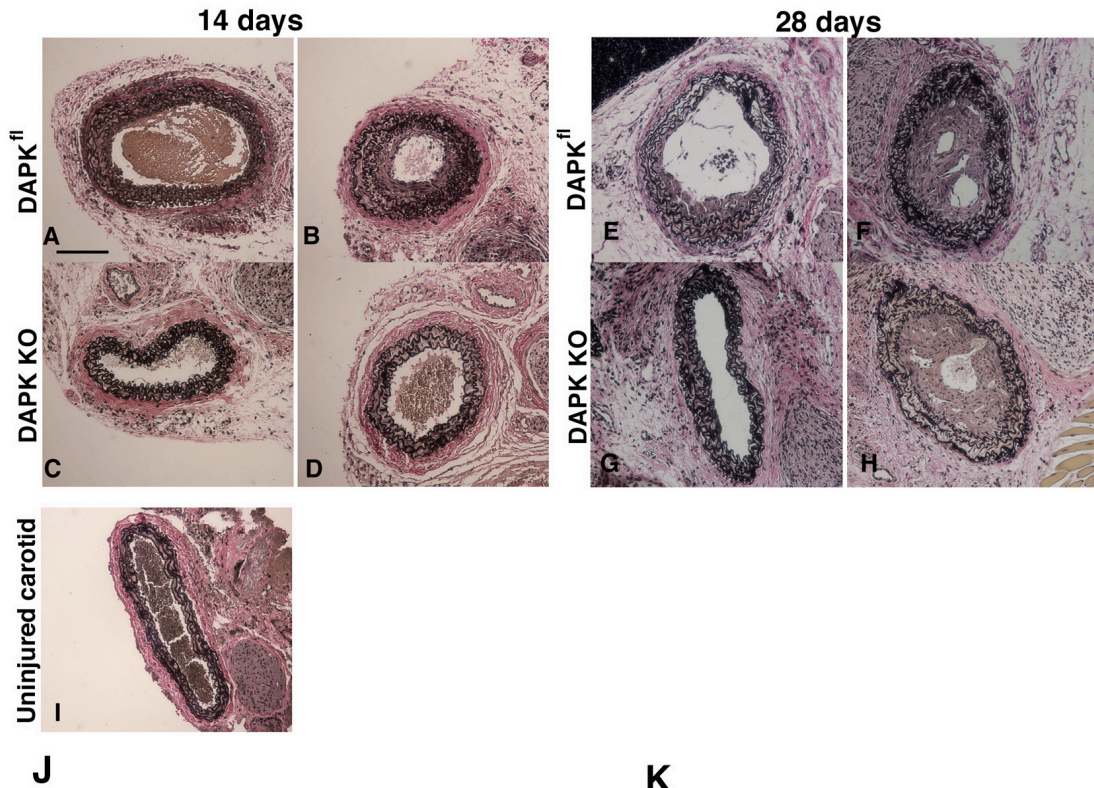
Figure 19: DAPK $^{-/-}$ mice exhibit less medial response to carotid injury after 14d.

A-H: Representative paraffin sections of injured arteries from DAPK^{fl} and DAPK$^{-/-}$ mice after fixation and staining with Verhoeff-Van Gieson which stains the elastic laminae black. A, B, C, D: 14 days after injury; E, F, G, H: 28 days after injury. I: Uninjured control artery. A, B, E, F are arteries from DAPK^{fl} mice; C, D, G, H are arteries from DAPK $^{-/-}$ mice (denoted DAPK KO). Scale bar in panel A shows 100 μm. J – K: Using ImageJ software, area of the medial smooth muscle layers

or the ratio of neointimal area (area of non-blood cell growth in lumen inside of inner elastic lamina) to the media area was measured, calculated, and graphed. Medial smooth muscle was defined as the area between the inner and outer elastic lamina. The numbers of arteries examined were: n=12 for 14 days DAPK^{fl} and DAPK KO; n=10 for 28d DAPK ^{fl} and n=9 for 28d DAPK KO. Duplicate sections were measured for each mouse. *p=0.034, DAPK^{fl} vs. DAPK KO, 14d post-injury.

Table 2: Primers used for RT-PCR

Primer name		Sequence (5' to 3')
Mo DAPK (exon 4)	Forward	TCATTCTGATCCTGGAGCTTG
	Reverse	TGCCTCCTCTTCAGTCAGAGA
Mo HPRT	Forward	TGGCCCTCTGTGTGCTCAA
	Reverse	TGATCATTACAGTAGCTCTTCAGTCTGA
Mo MMP9	Forward	CCTGAAAACCTCCAACCTCA
	Reverse	GGTGTAACCATAGCGGTACAAGT

Table 3: Primers used for genotyping and Southern blot probe template

Primer name	Sequence (5' to 3')
P1	TGCTTACTGTCTGGCAGTGG
P2	GCTTCCTCGTGCTTTACGGTATC
P3	TCTGTCCCCTCGTTTGTGAATG
P4	CAGGTGCCTCAGTTTCTCTTGG
P5	ATAGGAGCACAGCCCGTCTTGACAG
P6	TGGACGTAAACTCCTCTTCAGACCTG
P7	GCATTGAGCACCTTCCTTCACAC
P8	CGGAGCATTTCAGATGGCACTG
Southern probe forward	GAAGGAAGGGTTGAGAGAGTTGC
Southern probe reverse	CCAAGTTTGAGACAAGGCAGAGTC

Table 4: Frequency of genotypes observed

Line 244

244 (+/- x +/-)	DAPK +/+	DAPK+/-	DAPK -/-
Males	12 (27%)	27 (60%)	6 (13%)
Females	9 (22.5%)	19 (47.5%)	12 (30%)
Combined	21 (25%)	46 (54%)	18 (21%)
P value combined	0.67		
P value males	0.18		
P value females	0.76		

Line 315

315 (+/- x -/-)	DAPK +/-	DAPK -/-
Males	17 (57%)	13 (43%)
Females	15 (56%)	12 (44%)
Combined	32 (56%)	25 (44%)
P value combined	0.35	
P value males	0.47	
P value females	0.67	

Chapter IV: Future Studies and Conclusions

The results presented in the previous two chapters point to a role for DAPK in regulation of smooth muscle signaling. **Chapter II** focused on the regulation of MMP9 expression by modulating p65 activity in primary human coronary smooth muscle cells, and **Chapter III** presented studies using a newly generated DAPK$^{-/-}$ mouse. Examination of this mouse model revealed that DAPK promotes MMP9 expression and development of thickened media in a carotid injury model. Future studies will be delineated in this chapter to advance our understanding of the role of DAPK has on the physiology and pathology of smooth muscle and other tissues.

In **Chapter II**, results showed that DAPK negatively regulates levels of p65 phosphoS536. Using a phosphomimetic mutant p65 S536D, we showed that this phosphorylated form of p65 increases the NF-κB activity, and that the inhibitory effect of DAPK requires p65 to modulate MMP9 expression levels. Further studies are needed to confirm that DAPK depletion leads to increased binding of p65 phosphoS536 on the MMP9 and VCAM1 promoters. Chromatin immunoprecipitation assays should be used to examine the binding of p65 to endogenous promoters in control and DAPK-depleted HCASMC; increased binding of p65 phosphoS536 to the MMP9 and VCAM1 promoters is expected when DAPK is depleted from HCASMC. Other NF-κB regulated promoters that are not responsive to DAPK depletion (IL-8 and TNFα, data not shown) should be used as negative controls. In addition, the role of p65 partner NF-κB1/p50 in the transcription of MMP9 and VCAM1 should be explored to determine if its binding is also affected by DAPK depletion.

DAPK depletion results in increased p65 phosphoS536 via an unknown mechanism. There are several kinases that can phosphorylate p65 at S536, including IκKα/β and RSK. There was no increase in the active forms of IκKα/β in DAPK-depleted HCASMC, leading to the hypothesis that perhaps dephosphorylation of p65 was affected in these cells. PP2A has been previously

shown to both bind DAPK and also to dephosphorylate p65 phosphoS536. This ser/thr phosphatase is also partially localized to the nucleus in HCASMC (data not shown). Thus, it is possible that DAPK and PP2A are part of a complex that regulates the phosphorylation status of nuclear p65. Future studies should focus on determining if DAPK, PP2A and p65 form a complex, and if DAPK depletion leads to disruption of the PP2A/p65 complex. Alternatively, another binding partner of DAPK might be mediating the effect on p65. DAPK has also been shown to bind to Mib1, an E3 ubiquitin ligase. Previous studies have shown that p65 phosphoS536 is specifically targeted for degradation by the nuclear proteasome (72). Depletion of DAPK could disrupt the ubiquitination of p65 by Mib1; future studies should focus on determining if Mib1 can ubiquitinate p65 *in vitro* and *in vivo*, and whether or not Mib1 and p65 interact. The levels of p65 phosphoS536 phosphorylation and turnover are likely to be tightly regulated because p65 phosphoS536 does not bind IkBα (10, 13). This inhibitor of NF-κB signaling is responsible for maintaining p65 in the cytoplasm; thus, alternative mechanisms for terminating and regulating NF-κB signaling on promoters that bind p65 phosphoS536 are likely important and not well defined. Identification of the specific effect that DAPK has upon regulation of p65 phosphoS536 will further the knowledge in this field.

Another finding in **Chapter II** was that DAPK is localized to the nucleus. This finding was based on cell fractionation of HCASMC, and has been also found to be true for other cell line such as HeLa and 293HEK. Further studies to determine the regulation of DAPK nuclear localization are needed, such as characterization of sequences in DAPK that regulate its nuclear localization. One such highly basic amino acid sequence is located within the kinase domain of DAPK and site directed mutagenesis could be used to alter these residues and determine if nuclear localization was blocked.

Chapter III showed that the deletion of DAPK *in vivo* has a different effect on MMP9 than was shown in **Chapter II**. In normal aortic, carotid artery, or hepatic tissue from DAPK^fl/fl and DAPK^-/- mice, there was no difference in MMP9

mRNA or protein expression. Reduced levels of MMP9 were found at 7 days following ligation of the carotid artery in the small sample size examined. The sample size in this study should be expanded, and also data for MMP9 mRNA levels determined for the 7 day post-injury time point. After verification of the decreased MMP9 at 7 days in the DAPK KO mice, the reasons for the different effect that low DAPK levels have on MMP9 expression should be explored. The carotid artery is a complex environment, and more than one cell type likely contributes to the MMP9 levels produced in response to vascular injury, including SMC and macrophages. Further studies need to be done to determine which cells are primarily responsible for the production of MMP9 mRNA in the carotid artery ligation. It is also possible that the differences we observe are due to unique properties of coronary artery smooth muscle cells, as compared to aortic and carotid artery smooth muscle cells. Examination of mouse coronary arteries is difficult, so future studies should first focus on characterizing the role of DAPK in primary carotid smooth muscle cells from mouse and human tissue, and also in macrophages and immune cells. Depletion of DAPK in these other cell culture models should be done to determine what effect DAPK has on MMP9 expression. In addition, compensatory mechanisms are likely to be playing a role in masking the effects of the DAPK deletion and could explain the differences between acute depletion in cultured HCASMC compared to total sustained depletion in the mouse model. Further studies should examine if there are alterations in the NF-κB pathway to block the increased p65 phosphoS536 that may occur in the absence of DAPK.

Data presented in **Chapter III** indicates that DAPK$^{-/-}$ mice have decreased medial smooth muscle thickness at 14 days post injury. More studies should determine if these differences are due to changes in cell number, apoptosis, and proliferation. In **Chapter II**, staining of sections from ApoE$^{-/-}$ mice showed that DAPK expression is upregulated in atherosclerotic lesions from ApoE$^{-/-}$ mice that have been fed a high-fat diet. Double-knockout mice (DAPK$^{-/-}$; ApoE$^{-/-}$) should be

generated to determine if the increased DAPK contributes to the generation of atheromas.

The DAPK$^{-/-}$ mice were generated from a mouse that contained loxP sites around DAPK exon 4. These mice can be used in the future to generate tissue specific knockout mice in an unlimited number of studies to determine the effect of DAPK on specific cell types, such as endothelial cells, smooth muscle cells, immune cells, and other cell types, in both normal and injured arteries. Studies in nonvascular, DAPK-expressing tissues could also be undertaken using other Cre deleter mice. Because the deletion of DAPK is likely inducing compensatory changes to ensure the animals' survival, use of an inducible Cre system would allow for temporal control of DAPK deletion after the animals reach maturity. This strategy could reveal more effects of the loss of DAPK.

In conclusion, results presented here highlight roles for DAPK in vascular smooth muscle, both in human coronary artery smooth muscle cells and *in vivo* in the mouse carotid artery ligation model. DAPK levels were increased in the smooth muscle cells in two mouse models of vascular pathology. In the HCASMC, reduced DAPK levels led to increased cell migration and MMP9 expression. The mechanism behind the *in vitro* upregulation of MMP9 was identified, and we found that reduced DAPK leads to increased phosphorylated p65, which has more NF-κB activity on the MMP9 promoter. DAPK also plays a role in vascular pathology *in vivo*; in the DAPK$^{-/-}$ mice there was a reduced medial response to ligation of the carotid artery, and also less MMP9 expression. Thus, depending on the context and possibly cell type, DAPK plays different roles in regulation of cellular signaling that determines the amount of MMP9 produced by cells. In conclusion, DAPK plays a complex role in the regulation of vascular smooth muscle signaling.

References

1. Allayee, H., A. Ghazalpour, and A. J. Lusis. 2003. Using mice to dissect genetic factors in atherosclerosis. Arterioscler Thromb Vasc Biol 23:1501-9.

2. Anjum, R., P. P. Roux, B. A. Ballif, S. P. Gygi, and J. Blenis. 2005. The tumor suppressor DAP kinase is a target of RSK-mediated survival signaling. Curr Biol 15:1762-7.

3. Annabi, B., D. Shedid, P. Ghosn, R. L. Kenigsberg, R. R. Desrosiers, M. W. Bojanowski, E. Beaulieu, E. Nassif, R. Moumdjian, and R. Beliveau. 2002. Differential regulation of matrix metalloproteinase activities in abdominal aortic aneurysms. J Vasc Surg 35:539-46.

4. Barrett, T. B., and E. P. Benditt. 1988. Platelet-derived growth factor gene expression in human atherosclerotic plaques and normal artery wall. Proc Natl Acad Sci U S A 85:2810-4.

5. Betsuyaku, T., Y. Fukuda, W. C. Parks, J. M. Shipley, and R. M. Senior. 2000. Gelatinase B is required for alveolar bronchiolization after intratracheal bleomycin. Am J Pathol 157:525-35.

6. Bialik, S., H. Berissi, and A. Kimchi. 2008. A high throughput proteomics screen identifies novel substrates of death-associated protein kinase. Mol Cell Proteomics 7:1089-98.

7. Bialik, S., A. R. Bresnick, and A. Kimchi. 2004. DAP-kinase-mediated morphological changes are localization dependent and involve myosin-II phosphorylation. Cell Death Differ 11:631-44.

8. Bialik, S., and A. Kimchi. 2010. Lethal weapons: DAP-kinase, autophagy and cell death: DAP-kinase regulates autophagy. Curr Opin Cell Biol 22:199-205.

9. Bialik, S., and A. Kimchi. 2006. The death-associated protein kinases: structure, function, and beyond. Annu Rev Biochem 75:189-210.

10. Bohuslav, J., L. F. Chen, H. Kwon, Y. Mu, and W. C. Greene. 2004. p53 induces NF-kappaB activation by an IkappaB kinase-independent mechanism involving phosphorylation of p65 by ribosomal S6 kinase 1. J Biol Chem 279:26115-25.

11. Bottger, B. A., U. Hedin, S. Johansson, and J. Thyberg. 1989. Integrin-type fibronectin receptors of rat arterial smooth muscle cells: isolation, partial characterization and role in cytoskeletal organization and control of differentiated properties. Differentiation 41:158-67.

12. Braun, M., P. Pietsch, K. Schror, G. Baumann, and S. B. Felix. 1999. Cellular adhesion molecules on vascular smooth muscle cells. Cardiovasc Res 41:395-401.

13. Buss, H., A. Dorrie, M. L. Schmitz, E. Hoffmann, K. Resch, and M. Kracht. 2004. Constitutive and interleukin-1-inducible phosphorylation of p65 NF-{kappa}B at serine 536 is mediated by multiple protein kinases including I{kappa}B kinase (IKK)-{alpha}, IKK{beta}, IKK{epsilon}, TRAF family member-associated (TANK)-binding kinase 1 (TBK1), and an unknown kinase and couples p65 to TATA-binding protein-associated factor II31-mediated interleukin-8 transcription. J Biol Chem 279:55633-43.

14. Cabrera, S., M. Gaxiola, J. L. Arreola, R. Ramirez, P. Jara, J. D'Armiento, T. Richards, M. Selman, and A. Pardo. 2007. Overexpression of MMP9 in macrophages attenuates pulmonary fibrosis induced by bleomycin. Int J Biochem Cell Biol 39:2324-38.

15. Cai, Q., L. Lanting, and R. Natarajan. 2004. Growth factors induce monocyte binding to vascular smooth muscle cells: implications for monocyte retention in atherosclerosis. Am J Physiol Cell Physiol 287:C707-14.

16. Cai, Q., L. Lanting, and R. Natarajan. 2004. Interaction of monocytes with vascular smooth muscle cells regulates monocyte survival and differentiation through distinct pathways. Arterioscler Thromb Vasc Biol 24:2263-70.

17. Camejo, G., G. Fager, B. Rosengren, E. Hurt-Camejo, and G. Bondjers. 1993. Binding of low density lipoproteins by proteoglycans synthesized by proliferating and quiescent human arterial smooth muscle cells. J Biol Chem 268:14131-7.

18. Campbell, J. H., and G. R. Campbell. 1994. The role of smooth muscle cells in atherosclerosis. Curr Opin Lipidol 5:323-30.

19. Chait, A., and T. N. Wight. 2000. Interaction of native and modified low-density lipoproteins with extracellular matrix. Curr Opin Lipidol 11:457-63.

20. Chandrasekar, B., S. Mummidi, L. Mahimainathan, D. N. Patel, S. R. Bailey, S. Z. Imam, W. C. Greene, and A. J. Valente. 2006. Interleukin-18-induced human coronary artery smooth muscle cell migration is dependent on NF-kappaB- and AP-1-mediated matrix metalloproteinase-9 expression and is inhibited by atorvastatin. J Biol Chem 281:15099-109.

21. Chang, M. Y., S. Potter-Perigo, C. Tsoi, A. Chait, and T. N. Wight. 2000. Oxidized low density lipoproteins regulate synthesis of monkey aortic smooth muscle cell proteoglycans that have enhanced native low density lipoprotein binding properties. J Biol Chem 275:4766-73.

22. Chen, C. H., W. J. Wang, J. C. Kuo, H. C. Tsai, J. R. Lin, Z. F. Chang, and R. H. Chen. 2005. Bidirectional signals transduced by DAPK-ERK interaction promote the apoptotic effect of DAPK. EMBO J 24:294-304.

23. Chen, L. F., and W. C. Greene. 2004. Shaping the nuclear action of NF-kappaB. Nat Rev Mol Cell Biol 5:392-401.

24. Chen, L. F., S. A. Williams, Y. Mu, H. Nakano, J. M. Duerr, L. Buckbinder, and W. C. Greene. 2005. NF-kappaB RelA phosphorylation regulates RelA acetylation. Mol Cell Biol 25:7966-75.

25. Cho, A., J. Graves, and M. A. Reidy. 2000. Mitogen-activated protein kinases mediate matrix metalloproteinase-9 expression in vascular smooth muscle cells. Arterioscler Thromb Vasc Biol 20:2527-32.

26. Cho, A., and M. A. Reidy. 2002. Matrix metalloproteinase-9 is necessary for the regulation of smooth muscle cell replication and migration after arterial injury. Circ Res 91:845-51.

27. Chuang, Y. T., L. W. Fang, M. H. Lin-Feng, R. H. Chen, and M. Z. Lai. 2008. The tumor suppressor death-associated protein kinase targets to TCR-stimulated NF-kappa B activation. J Immunol 180:3238-49.

28. Cohen, O., E. Feinstein, and A. Kimchi. 1997. DAP-kinase is a Ca2+/calmodulin-dependent, cytoskeletal-associated protein kinase, with cell death-inducing functions that depend on its catalytic activity. EMBO J 16:998-1008.

29. Corjay, M. H., M. M. Thompson, K. R. Lynch, and G. K. Owens. 1989. Differential effect of platelet-derived growth factor- versus serum-induced growth on smooth muscle alpha-actin and nonmuscle beta-actin mRNA expression in cultured rat aortic smooth muscle cells. J Biol Chem 264:10501-6.

30. Deiss, L. P., E. Feinstein, H. Berissi, O. Cohen, and A. Kimchi. 1995. Identification of a novel serine/threonine kinase and a novel 15-kD protein as potential mediators of the gamma interferon-induced cell death. Genes Dev 9:15-30.

31. Doran, A. C., N. Meller, and C. A. McNamara. 2008. Role of smooth muscle cells in the initiation and early progression of atherosclerosis. Arterioscler Thromb Vasc Biol 28:812-9.

32. Eisenberg-Lerner, A., and A. Kimchi. 2007. DAP kinase regulates JNK signaling by binding and activating protein kinase D under oxidative stress. Cell Death Differ.

33. Endres, M., U. Laufs, H. Merz, and M. Kaps. 1997. Focal expression of intercellular adhesion molecule-1 in the human carotid bifurcation. Stroke 28:77-82.

34. Falk, E. 2006. Pathogenesis of atherosclerosis. J Am Coll Cardiol 47:C7-12.

35. Fitzgerald, M., I. P. Hayward, A. C. Thomas, G. R. Campbell, and J. H. Campbell. 1999. Matrix metalloproteinase can facilitate the heparanase-induced promotion of phenotype change in vascular smooth muscle cells. Atherosclerosis 145:97-106.

36. Fraser, J. A., and T. R. Hupp. 2007. Chemical genetics approach to identify peptide ligands that selectively stimulate DAPK-1 kinase activity. Biochemistry 46:2655-73.

37. Frutkin, A. D., H. Shi, G. Otsuka, and D. A. Dichek. 2007. Targeted rearrangement of floxed alleles in smooth muscle cells in vivo. Circ Res 101:e124-5.

38. Galis, Z. S., C. Johnson, D. Godin, R. Magid, J. M. Shipley, R. M. Senior, and E. Ivan. 2002. Targeted disruption of the matrix metalloproteinase-9 gene impairs smooth muscle cell migration and geometrical arterial remodeling. Circ Res 91:852-9.

39. Ghosh, C. C., S. Ramaswami, A. Juvekar, H. Y. Vu, L. Galdieri, D. Davidson, and I. Vancurova. 2010. Gene-specific repression of proinflammatory cytokines in stimulated human macrophages by nuclear IkappaBalpha. J Immunol 185:3685-93.

40. Godin, D., E. Ivan, C. Johnson, R. Magid, and Z. S. Galis. 2000. Remodeling of carotid artery is associated with increased expression of matrix metalloproteinases in mouse blood flow cessation model. Circulation 102:2861-6.

41. Gough, P. J., I. G. Gomez, P. T. Wille, and E. W. Raines. 2006. Macrophage expression of active MMP-9 induces acute plaque disruption in apoE-deficient mice. J Clin Invest 116:59-69.

42. Gozuacik, D., S. Bialik, T. Raveh, G. Mitou, G. Shohat, H. Sabanay, N. Mizushima, T. Yoshimori, and A. Kimchi. 2008. DAP-kinase is a mediator of endoplasmic reticulum stress-induced caspase activation and autophagic cell death. Cell Death Differ 15:1875-86.

43. Gupta, S., A. M. Pablo, X. Jiang, N. Wang, A. R. Tall, and C. Schindler. 1997. IFN-gamma potentiates atherosclerosis in ApoE knock-out mice. J Clin Invest 99:2752-61.

44. Hanks, S. K., and T. Hunter. 1995. Protein kinases 6. The eukaryotic protein kinase superfamily: kinase (catalytic) domain structure and classification. FASEB J 9:576-96.

45. Hautmann, M. B., C. S. Madsen, and G. K. Owens. 1997. A transforming growth factor beta (TGFbeta) control element drives TGFbeta-induced stimulation of smooth muscle alpha-actin gene expression in concert with two CArG elements. J Biol Chem 272:10948-56.

46. Hayden, M. S., and S. Ghosh. 2008. Shared principles in NF-kappaB signaling. Cell 132:344-62.

47. Hoberg, J. E., A. E. Popko, C. S. Ramsey, and M. W. Mayo. 2006. IkappaB kinase alpha-mediated derepression of SMRT potentiates acetylation of RelA/p65 by p300. Mol Cell Biol 26:457-71.

48. Houle, F., A. Poirier, J. Dumaresq, and J. Huot. 2007. DAP kinase mediates the phosphorylation of tropomyosin-1 downstream of the ERK pathway, which regulates the formation of stress fibers in response to oxidative stress. J Cell Sci 120:3666-77.

49. Hu, J., M. Haseebuddin, M. Young, and N. H. Colburn. 2005. Suppression of p65 phosphorylation coincides with inhibition of IkappaBalpha polyubiquitination and degradation. Mol Carcinog 44:274-84.

50. Hu, J., H. Nakano, H. Sakurai, and N. H. Colburn. 2004. Insufficient p65 phosphorylation at S536 specifically contributes to the lack of NF-kappaB activation and transformation in resistant JB6 cells. Carcinogenesis 25:1991-2003.

51. Huang, B., X. D. Yang, A. Lamb, and L. F. Chen. 2010. Posttranslational modifications of NF-kappaB: another layer of regulation for NF-kappaB signaling pathway. Cell Signal 22:1282-90.

52. Ikari, Y., B. M. McManus, J. Kenyon, and S. M. Schwartz. 1999. Neonatal intima formation in the human coronary artery. Arterioscler Thromb Vasc Biol 19:2036-40.

53. Inbal, B., S. Bialik, I. Sabanay, G. Shani, and A. Kimchi. 2002. DAP kinase and DRP-1 mediate membrane blebbing and the formation of autophagic vesicles during programmed cell death. J Cell Biol 157:455-68.

54. Inbal, B., O. Cohen, S. Polak-Charcon, J. Kopolovic, E. Vadai, L. Eisenbach, and A. Kimchi. 1997. DAP kinase links the control of apoptosis to metastasis. Nature 390:180-4.

55. Ishibashi, S., M. S. Brown, J. L. Goldstein, R. D. Gerard, R. E. Hammer, and J. Herz. 1993. Hypercholesterolemia in low density lipoprotein receptor knockout mice and its reversal by adenovirus-mediated gene delivery. J Clin Invest 92:883-93.

56. Iyer, V., K. Pumiglia, and C. M. DiPersio. 2005. Alpha3beta1 integrin regulates MMP-9 mRNA stability in immortalized keratinocytes: a novel mechanism of integrin-mediated MMP gene expression. J Cell Sci 118:1185-95.

57. Jang, Y., A. M. Lincoff, E. F. Plow, and E. J. Topol. 1994. Cell adhesion molecules in coronary artery disease. J Am Coll Cardiol 24:1591-601.

58. Jin, Y., E. K. Blue, S. Dixon, L. Hou, R. B. Wysolmerski, and P. J. Gallagher. 2001. Identification of a new form of death-associated protein kinase that promotes cell survival. J Biol Chem 276:39667-78.

59. Jin, Y., E. K. Blue, S. Dixon, Z. Shao, and P. J. Gallagher. 2002. A death-associated protein kinase (DAPK)-interacting protein, DIP-1, is an E3 ubiquitin ligase that promotes tumor necrosis factor-induced apoptosis and regulates the cellular levels of DAPK. J Biol Chem 277:46980-6.

60. Jin, Y., E. K. Blue, and P. J. Gallagher. 2006. Control of death-associated protein kinase (DAPK) activity by phosphorylation and proteasomal degradation. J Biol Chem 281:39033-40.

61. Jin, Y., and P. J. Gallagher. 2003. Antisense depletion of death-associated protein kinase promotes apoptosis. J Biol Chem 278:51587-93.

62. Johnson, C., and Z. S. Galis. 2004. Matrix metalloproteinase-2 and -9 differentially regulate smooth muscle cell migration and cell-mediated collagen organization. Arterioscler Thromb Vasc Biol 24:54-60.

63. Kishino, M., K. Yukawa, K. Hoshino, A. Kimura, N. Shirasawa, H. Otani, T. Tanaka, K. Owada-Makabe, Y. Tsubota, M. Maeda, M. Ichinose, K. Takeda, S. Akira, and M. Mune. 2004. Deletion of the kinase domain in death-associated protein kinase attenuates tubular cell apoptosis in renal ischemia-reperfusion injury. J Am Soc Nephrol 15:1826-34.

64. Kissil, J. L., E. Feinstein, O. Cohen, P. A. Jones, Y. C. Tsai, M. A. Knowles, M. E. Eydmann, and A. Kimchi. 1997. DAP-kinase loss of expression in various carcinoma and B-cell lymphoma cell lines: possible implications for role as tumor suppressor gene. Oncogene 15:403-7.

65. Knowles, J. W., and N. Maeda. 2000. Genetic modifiers of atherosclerosis in mice. Arterioscler Thromb Vasc Biol 20:2336-45.

66. Knox, J. B., G. K. Sukhova, A. D. Whittemore, and P. Libby. 1997. Evidence for altered balance between matrix metalloproteinases and their inhibitors in human aortic diseases. Circulation 95:205-12.

67. Koyama, N., M. G. Kinsella, T. N. Wight, U. Hedin, and A. W. Clowes. 1998. Heparan sulfate proteoglycans mediate a potent inhibitory signal for migration of vascular smooth muscle cells. Circ Res 83:305-13.

68. Ku, D. N., D. P. Giddens, C. K. Zarins, and S. Glagov. 1985. Pulsatile flow and atherosclerosis in the human carotid bifurcation. Positive correlation between plaque location and low oscillating shear stress. Arteriosclerosis 5:293-302.

69. Kumar, A., and V. Lindner. 1997. Remodeling with neointima formation in the mouse carotid artery after cessation of blood flow. Arterioscler Thromb Vasc Biol 17:2238-44.

70. Kuo, J. C., J. R. Lin, J. M. Staddon, H. Hosoya, and R. H. Chen. 2003. Uncoordinated regulation of stress fibers and focal adhesions by DAP kinase. J Cell Sci 116:4777-90.

71. Kuo, J. C., W. J. Wang, C. C. Yao, P. R. Wu, and R. H. Chen. 2006. The tumor suppressor DAPK inhibits cell motility by blocking the integrin-mediated polarity pathway. J Cell Biol 172:619-31.

72. Lawrence, T., M. Bebien, G. Y. Liu, V. Nizet, and M. Karin. 2005. IKKalpha limits macrophage NF-kappaB activation and contributes to the resolution of inflammation. Nature 434:1138-43.

73. Leber, T. M., and F. R. Balkwill. 1997. Zymography: a single-step staining method for quantitation of proteolytic activity on substrate gels. Anal Biochem 249:24-8.

74. Lessner, S. M., D. E. Martinson, and Z. S. Galis. 2004. Compensatory vascular remodeling during atherosclerotic lesion growth depends on matrix metalloproteinase-9 activity. Arterioscler Thromb Vasc Biol 24:2123-9.

75. Li, H., M. W. Freeman, and P. Libby. 1995. Regulation of smooth muscle cell scavenger receptor expression in vivo by atherogenic diets and in vitro by cytokines. J Clin Invest 95:122-33.

76. Li, H., J. Liang, D. H. Castrillon, R. A. DePinho, E. N. Olson, and Z. P. Liu. 2007. FoxO4 regulates tumor necrosis factor alpha-directed smooth muscle cell migration by activating matrix metalloproteinase 9 gene transcription. Mol Cell Biol 27:2676-86.

77. Li, X., V. Van Putten, F. Zarinetchi, M. E. Nicks, S. Thaler, L. E. Heasley, and R. A. Nemenoff. 1997. Suppression of smooth-muscle alpha-actin expression by platelet-derived growth factor in vascular smooth-muscle cells involves Ras and cytosolic phospholipase A2. Biochem J 327 (Pt 3):709-16.

78. Lin, Y., T. R. Hupp, and C. Stevens. 2010. Death-associated protein kinase (DAPK) and signal transduction: additional roles beyond cell death. FEBS J 277:48-57.

79. Lindner, V., J. Fingerle, and M. A. Reidy. 1993. Mouse model of arterial injury. Circ Res 73:792-6.

80. Lusis, A. J. 2000. Atherosclerosis. Nature 407:233-41.

81. Martinet, W., D. M. Schrijvers, G. R. De Meyer, J. Thielemans, M. W. Knaapen, A. G. Herman, and M. M. Kockx. 2002. Gene expression profiling of apoptosis-related genes in human atherosclerosis: upregulation of death-associated protein kinase. Arterioscler Thromb Vasc Biol 22:2023-9.

82. Mason, D. P., R. D. Kenagy, D. Hasenstab, D. F. Bowen-Pope, R. A. Seifert, S. Coats, S. M. Hawkins, and A. W. Clowes. 1999. Matrix metalloproteinase-9 overexpression enhances vascular smooth muscle cell migration and alters remodeling in the injured rat carotid artery. Circ Res 85:1179-85.

83. Moon, S. K., B. Y. Cha, and C. H. Kim. 2004. ERK1/2 mediates TNF-alpha-induced matrix metalloproteinase-9 expression in human vascular smooth muscle cells via the regulation of NF-kappaB and AP-1: Involvement of the ras dependent pathway. J Cell Physiol 198:417-27.

84. Moses, H. L., E. Y. Yang, and J. A. Pietenpol. 1990. TGF-beta stimulation and inhibition of cell proliferation: new mechanistic insights. Cell 63:245-7.

85. Natoli, G., S. Saccani, D. Bosisio, and I. Marazzi. 2005. Interactions of NF-kappaB with chromatin: the art of being at the right place at the right time. Nat Immunol 6:439-45.

86. Newby, A. C. 2005. Dual role of matrix metalloproteinases (matrixins) in intimal thickening and atherosclerotic plaque rupture. Physiol Rev 85:1-31.

87. Newby, A. C. 2006. Matrix metalloproteinases regulate migration, proliferation, and death of vascular smooth muscle cells by degrading matrix and non-matrix substrates. Cardiovasc Res 69:614-24.

88. Ni, W., K. Egashira, S. Kitamoto, C. Kataoka, M. Koyanagi, S. Inoue, K. Imaizumi, C. Akiyama, K. I. Nishida, and A. Takeshita. 2001. New anti-monocyte chemoattractant protein-1 gene therapy attenuates atherosclerosis in apolipoprotein E-knockout mice. Circulation 103:2096-101.

89. O'Brien, K. D., M. D. Allen, T. O. McDonald, A. Chait, J. M. Harlan, D. Fishbein, J. McCarty, M. Ferguson, K. Hudkins, C. D. Benjamin, and et al. 1993. Vascular cell adhesion molecule-1 is expressed in human coronary atherosclerotic plaques. Implications for the mode of progression of advanced coronary atherosclerosis. J Clin Invest 92:945-51.

90. Owens, G. K., M. S. Kumar, and B. R. Wamhoff. 2004. Molecular regulation of vascular smooth muscle cell differentiation in development and disease. Physiol Rev 84:767-801.

91. Paigen, B., A. Morrow, C. Brandon, D. Mitchell, and P. Holmes. 1985. Variation in susceptibility to atherosclerosis among inbred strains of mice. Atherosclerosis 57:65-73.

92. Pan, J. H., G. K. Sukhova, J. T. Yang, B. Wang, T. Xie, H. Fu, Y. Zhang, A. R. Satoskar, J. R. David, C. N. Metz, R. Bucala, K. Fang, D. I. Simon, H. A. Chapman, P. Libby, and G. P. Shi. 2004. Macrophage migration inhibitory factor deficiency impairs atherosclerosis in low-density lipoprotein receptor-deficient mice. Circulation 109:3149-53.

93. Pidkovka, N. A., O. A. Cherepanova, T. Yoshida, M. R. Alexander, R. A. Deaton, J. A. Thomas, N. Leitinger, and G. K. Owens. 2007. Oxidized phospholipids induce phenotypic switching of vascular smooth muscle cells in vivo and in vitro. Circ Res 101:792-801.

94. Piedrahita, J. A., S. H. Zhang, J. R. Hagaman, P. M. Oliver, and N. Maeda. 1992. Generation of mice carrying a mutant apolipoprotein E gene inactivated by gene targeting in embryonic stem cells. Proc Natl Acad Sci U S A 89:4471-5.

95. Plump, A. S., J. D. Smith, T. Hayek, K. Aalto-Setala, A. Walsh, J. G. Verstuyft, E. M. Rubin, and J. L. Breslow. 1992. Severe hypercholesterolemia and atherosclerosis in apolipoprotein E-deficient mice created by homologous recombination in ES cells. Cell 71:343-53.

96. Raines, E. W., and N. Ferri. 2005. Thematic review series: The immune system and atherogenesis. Cytokines affecting endothelial and smooth muscle cells in vascular disease. J Lipid Res 46:1081-92.

97. Reusch, P., H. Wagdy, R. Reusch, E. Wilson, and H. E. Ives. 1996. Mechanical strain increases smooth muscle and decreases nonmuscle myosin expression in rat vascular smooth muscle cells. Circ Res 79:1046-53.

98. Rong, J. X., M. Shapiro, E. Trogan, and E. A. Fisher. 2003. Transdifferentiation of mouse aortic smooth muscle cells to a macrophage-like state after cholesterol loading. Proc Natl Acad Sci U S A 100:13531-6.

99. Ross, R. 1993. The pathogenesis of atherosclerosis: a perspective for the 1990s. Nature 362:801-9.

100. Roy, J., P. K. Tran, P. Religa, M. Kazi, B. Henderson, K. Lundmark, and U. Hedin. 2002. Fibronectin promotes cell cycle entry in smooth muscle cells in primary culture. Exp Cell Res 273:169-77.

101. Ruan, X. Z., J. F. Moorhead, J. L. Tao, K. L. Ma, D. C. Wheeler, S. H. Powis, and Z. Varghese. 2006. Mechanisms of dysregulation of low-density lipoprotein receptor expression in vascular smooth muscle cells by inflammatory cytokines. Arterioscler Thromb Vasc Biol 26:1150-5.

102. Sakurai, H., H. Chiba, H. Miyoshi, T. Sugita, and W. Toriumi. 1999. IkappaB kinases phosphorylate NF-kappaB p65 subunit on serine 536 in the transactivation domain. J Biol Chem 274:30353-6.

103. Sakurai, H., S. Suzuki, N. Kawasaki, H. Nakano, T. Okazaki, A. Chino, T. Doi, and I. Saiki. 2003. Tumor necrosis factor-alpha-induced IKK phosphorylation of NF-kappaB p65 on serine 536 is mediated through the TRAF2, TRAF5, and TAK1 signaling pathway. J Biol Chem 278:36916-23.

104. Sasaki, C. Y., T. J. Barberi, P. Ghosh, and D. L. Longo. 2005. Phosphorylation of RelA/p65 on serine 536 defines an I{kappa}B{alpha}-independent NF-{kappa}B pathway. J Biol Chem 280:34538-47.

105. Sata, M., Y. Maejima, F. Adachi, K. Fukino, A. Saiura, S. Sugiura, T. Aoyagi, Y. Imai, H. Kurihara, K. Kimura, M. Omata, M. Makuuchi, Y. Hirata, and R. Nagai. 2000. A mouse model of vascular injury that induces rapid onset of medial cell apoptosis followed by reproducible neointimal hyperplasia. J Mol Cell Cardiol 32:2097-104.

106. Schumacher, A. M., J. P. Schavocky, A. V. Velentza, S. Mirzoeva, and D. M. Watterson. 2004. A calmodulin-regulated protein kinase linked to neuron survival is a substrate for the calmodulin-regulated death-associated protein kinase. Biochemistry 43:8116-24.

107. Schumacher, A. M., A. V. Velentza, D. M. Watterson, and J. Dresios. 2006. Death-associated protein kinase phosphorylates mammalian ribosomal protein S6 and reduces protein synthesis. Biochemistry 45:13614-21.

108. Shani, G., L. Marash, D. Gozuacik, S. Bialik, L. Teitelbaum, G. Shohat, and A. Kimchi. 2004. Death-associated protein kinase phosphorylates ZIP kinase, forming a unique kinase hierarchy to activate its cell death functions. Mol Cell Biol 24:8611-26.

109. Shohat, G., T. Spivak-Kroizman, O. Cohen, S. Bialik, G. Shani, H. Berrisi, M. Eisenstein, and A. Kimchi. 2001. The pro-apoptotic function of death-associated protein kinase is controlled by a unique inhibitory autophosphorylation-based mechanism. J Biol Chem 276:47460-7.

110. Stary, H. C. 2000. Natural history and histological classification of atherosclerotic lesions: an update. Arterioscler Thromb Vasc Biol 20:1177-8.

111. Stary, H. C., D. H. Blankenhorn, A. B. Chandler, S. Glagov, W. Insull, Jr., M. Richardson, M. E. Rosenfeld, S. A. Schaffer, C. J. Schwartz, W. D. Wagner, and et al. 1992. A definition of the intima of human arteries and of its atherosclerosis-prone regions. A report from the Committee on Vascular Lesions of the Council on Arteriosclerosis, American Heart Association. Arterioscler Thromb 12:120-34.

112. Stary, H. C., A. B. Chandler, S. Glagov, J. R. Guyton, W. Insull, Jr., M. E. Rosenfeld, S. A. Schaffer, C. J. Schwartz, W. D. Wagner, and R. W. Wissler. 1994. A definition of initial, fatty streak, and intermediate lesions of atherosclerosis. A report from the Committee on Vascular Lesions of the Council on Arteriosclerosis, American Heart Association. Arterioscler Thromb 14:840-56.

113. Su, B., S. Mitra, H. Gregg, S. Flavahan, M. A. Chotani, K. R. Clark, P. J. Goldschmidt-Clermont, and N. A. Flavahan. 2001. Redox regulation of vascular smooth muscle cell differentiation. Circ Res 89:39-46.

114. Thompson, J. S. 1969. Atheromata in an inbred strain of mice. J Atheroscler Res 10:113-22.

115. Thyberg, J., and A. Hultgardh-Nilsson. 1994. Fibronectin and the basement membrane components laminin and collagen type IV influence the phenotypic properties of subcultured rat aortic smooth muscle cells differently. Cell Tissue Res 276:263-71.

116. Tian, J. H., S. Das, and Z. H. Sheng. 2003. Ca2+-dependent phosphorylation of syntaxin-1A by the death-associated protein (DAP) kinase regulates its interaction with Munc18. J Biol Chem 278:26265-74.

117. Truett, G. E., P. Heeger, R. L. Mynatt, A. A. Truett, J. A. Walker, and M. L. Warman. 2000. Preparation of PCR-quality mouse genomic DNA with hot sodium hydroxide and tris (HotSHOT). Biotechniques 29:52, 54.

118. Tu, W., X. Xu, L. Peng, X. Zhong, W. Zhang, M. M. Soundarapandian, C. Balel, M. Wang, N. Jia, F. Lew, S. L. Chan, Y. Chen, and Y. Lu. 2010. DAPK1 interaction with NMDA receptor NR2B subunits mediates brain damage in stroke. Cell 140:222-34.

119. Van den Steen, P. E., P. Proost, A. Wuyts, J. Van Damme, and G. Opdenakker. 2000. Neutrophil gelatinase B potentiates interleukin-8 tenfold by aminoterminal processing, whereas it degrades CTAP-III, PF-4, and GRO-alpha and leaves RANTES and MCP-2 intact. Blood 96:2673-81.

120. Velentza, A. V., A. M. Schumacher, C. Weiss, M. Egli, and D. M. Watterson. 2001. A protein kinase associated with apoptosis and tumor suppression: structure, activity, and discovery of peptide substrates. J Biol Chem 276:38956-65.

121. Wang, W. J., J. C. Kuo, C. C. Yao, and R. H. Chen. 2002. DAP-kinase induces apoptosis by suppressing integrin activity and disrupting matrix survival signals. J Cell Biol 159:169-79.

122. Weninger, W. J., G. B. Muller, C. Reiter, S. Meng, and S. U. Rabl. 1999. Intimal hyperplasia of the infant parasellar carotid artery: a potential developmental factor in atherosclerosis and SIDS. Circ Res 85:970-5.

123. Widau, R. C., Y. Jin, S. A. Dixon, B. E. Wadzinski, and P. J. Gallagher. 2010. Protein phosphatase 2A (PP2A) holoenzymes regulate death-associated protein kinase (DAPK) in ceramide-induced anoikis. J Biol Chem 285:13827-38.

124. Woodside, K. J., A. Hernandez, F. W. Smith, X. Y. Xue, M. Hu, J. A. Daller, and G. C. Hunter. 2003. Differential gene expression in primary and recurrent carotid stenosis. Biochem Biophys Res Commun 302:509-14.

125. Xin, H. B., K. Y. Deng, M. Rishniw, G. Ji, and M. I. Kotlikoff. 2002. Smooth muscle expression of Cre recombinase and eGFP in transgenic mice. Physiol Genomics 10:211-5.

126. Xu, Q. 2004. Mouse models of arteriosclerosis: from arterial injuries to vascular grafts. Am J Pathol 165:1-10.

127. Yang, J., G. H. Fan, B. E. Wadzinski, H. Sakurai, and A. Richmond. 2001. Protein phosphatase 2A interacts with and directly dephosphorylates RelA. J Biol Chem 276:47828-33.

128. Zalckvar, E., H. Berissi, L. Mizrachy, Y. Idelchuk, I. Koren, M. Eisenstein, H. Sabanay, R. Pinkas-Kramarski, and A. Kimchi. 2009. DAP-kinase-mediated phosphorylation on the BH3 domain of beclin 1 promotes dissociation of beclin 1 from Bcl-XL and induction of autophagy. EMBO Rep 10:285-92.

129. Zhang, L., K. P. Nephew, and P. J. Gallagher. 2007. Regulation of death-associated protein kinase. Stabilization by HSP90 heterocomplexes. J Biol Chem 282:11795-804.

130. Zhang, S. H., R. L. Reddick, J. A. Piedrahita, and N. Maeda. 1992. Spontaneous hypercholesterolemia and arterial lesions in mice lacking apolipoprotein E. Science 258:468-71.

131. Zhou, J., E. K. Blue, G. Hu, and B. P. Herring. 2008. Thymine DNA glycosylase represses myocardin-induced smooth muscle cell differentiation by competing with serum response factor for myocardin binding. J Biol Chem 283:35383-92.

Curriculum Vitae

Emily Keller Blue

Education

8/04-12/10   *PhD, Cellular and Integrative Physiology*
              Minor: Diabetes and Obesity
              Indiana University, Indianapolis, IN
              Advisor: Dr. Patricia J. Gallagher
8/91-8/95   *BS Biochemistry with high distinction*
              Indiana University, Bloomington, IN

Research Experience

7/99-8/04   *Research Analyst*
              Indiana University School of Medicine, Indianapolis, IN
              Cellular and Integrative Physiology
              Lab: Dr. Patricia J. Gallagher
2/98-7/99   *Research Technician*
              Indiana University School of Medicine, Indianapolis, IN
4/96-10/97   *Biochemist*
              National Starch and Chemical Company, Bridgewater, NJ
              Natural Polymer Research
5/94-8/95   *Undergraduate Researcher*
              Indiana University, Bloomington, IN
              Department of Chemistry

Awards And Honors

IUPUI Dissertation Scholarship Award: 2010
American Heart Association Predoctoral Fellowship: 2008-2010
GK-12 Fellowship: 2008-2009
        NSF grant to IU School of Medicine (declined due to overlapping funding)
Sigma Xi Research Competition, 3rd place: June 2008
Diabetes and Obesity Fellowship: 2006-2008
        T32 Training Grant to Indiana University
Moenkhaus Graduate Physiology Fellowship: 2005-2006
        Cellular and Integrative Physiology, Indiana University School of Medicine
University Fellowship: 2004-2005
        Indiana University, Graduate School
Phi Beta Kappa, Indiana University
Golden Key National Honor Society, Indiana University
Honors in Chemistry, Indiana University

Publications

E.K. Blue , F. Li, D.A. Ingram, Jr., B.P. Herring, and P.J. Gallagher. DAPK blocks MMP9 expression in vascular smooth muscle cells via indirect regulation of NF-κB p65 phosphorylation. (*In preparation*)

K.M. Habegger, L. Tackett, L.N. Bell, M.Y. Awad, P.J. Gallagher, **E.K. Blue**, M. Sturek, M. A. Alloosh, H. O. Steinberg, R.V. Considine, and J.S. Elmendorf. Fatty Acid-Induced Plasma Membrane Cholesterol Accrual and Insulin Resistance. (*In revision*)

J. Zhou, **E.K. Blue**, G. Hu, & B.P. Herring. 2008. Thymine DNA glycosylase represses myocardin-induced smooth muscle cell differentiation by competing with SRF for myocardin binding. *J. Biol Chem*. 283:35383-92.

Y. Jin, **E.K. Blue**, and P.J. Gallagher. 2006. Control of death associated protein kinase (DAPK) activity by phosphorylation and proteasomal degradation. *J Biol Chem*. 281:39033-40.

E.K. Blue*, Z.M. Goeckeler*, Y. Jin, L. Hou, S.A. Dixon, B.P. Herring, R.B. Wysolmerski, and P.J. Gallagher. 2002. 220- and 130-kDa MLCKs have distinct tissue distributions and intracellular localization patterns. *Am J Physiol Cell Physiol*. 282:C451-60.

Y. Jin*, **E.K. Blue***, S. Dixon, Z. Shao, and P.J. Gallagher. 2002. A death-associated protein kinase (DAPK)-interacting protein, DIP-1, is an E3 ubiquitin ligase that promotes tumor necrosis factor-induced apoptosis and regulates the cellular levels of DAPK. *J Biol Chem*. 277:46980-6.

Y. Jin*, **E.K. Blue***, S. Dixon, L. Hou, R.B. Wysolmerski, and P.J. Gallagher. 2001. Identification of a new form of death-associated protein kinase that promotes cell survival. *J Biol Chem*. 276:39667-78.

P.J. Gallagher, Y. Jin, G. Killough, **E.K. Blue**, and V. Lindner. 2000. Alterations in expression of myosin and myosin light chain kinases in response to vascular injury. *Am J Physiol Cell Physiol*. 279:C1078-87.

W.L. Nowatzke, **E. Keller**, G. Koch, and J.P. Richardson. 1997. Transcription term-ination factor Rho is essential for Micrococcus luteus. *J Bacteriol*. 179:5238-40.

*Both authors made equal contributions to the work.

Abstracts

North American Vascular Biology Organization/Experimental Biology 2007: Blue, E.K. and Gallagher, P.J. "Role of DAP kinase in atherosclerosis and inflammation" (April 2007, Oral Presentation)

NAVBO Signaling in the Cardiovascular System Workshop: "DAPK: A Novel Mediator and Target of TGF-beta Signaling in Vascular Smooth Muscle" (September 2008, poster)

Meetings/Courses Attended

American Society for Cell Biology, December 1999

Experimental Biology, April 2001

Vasculata Vascular Biology Course (NAVBO), July 2004
American Diabetes Association, June 2005
IU Continuing Medical Education Grant Writing Workshop, October 2005
Preparing Future Faculty Program, December 2005-May 2008
Experimental Biology, April 2007
NAVBO Signaling in the Cardiovascular System Workshop, September 2008

Service
Tutor for Chemistry, Biology, and Math: IU School of Medicine/Crispus Attucks
Medical Magnet Program, 2009-2010
Cellular and Integrative Physiology Graduate Student Representative to Indiana
University School of Medicine (IUSM), 2006-2007
- Organizer and judging panelist: Student Travel Grant Competition: 2006-2007
- Physiology Department Seminar Committee, Student Representative: 2006-2007

IUSM Graduate Student Representative to campus-wide IUPUI Graduate Student
Organization: 2006-2007
- Judging panelist: IUPUI Campus-wide Educational Enhancement Grant Competition: 2006-2007

Professional Associations
North American Vascular Biology Organization, 2006-2009
American Academy for the Advancement of Science, 2007-2009
American Physiology Association, 2008-2009

Presentations
Departmental Research in Progress, January 2006, "A potential role for DAPK in vascular smooth muscle differentiation" (Oral Presentation)
Sigma Xi research competition, June 2006, "A potential role for DAPK in regulation of vascular smooth muscle differentiation" (Oral Presentation)
Indiana Center for Vascular Biology, September 2006, "Regulation of death-associated protein kinase (DAPK) expression in smooth muscle cells" (Poster)
Departmental Research in Progress, January 2007, "Potential roles for DAPK in vascular smooth muscle" (Oral Presentation)
North American Vascular Biology Organization/Experimental Biology 2007, April 2007, "Role of DAP kinase in atherosclerosis and inflammation" (Oral Presentation)
Departmental retreat, August 2007, "Role of DAPK in atherosclerosis and inflammation" (Oral Presentation)
Sigma Xi research competition, May 2008, "DAPK: A novel mediator and target of TGF-beta signaling in vascular smooth muscle" (Oral Presentation)

Departmental Research in Progress, August 2008, "DAPK, TGF-beta, and ECM: New roles for a kinase in vascular smooth muscle" (Oral Presentation)

Departmental Retreat, August 2008, "DAPK: A Novel Mediator and Target of TGF-beta Signaling in Vascular Smooth Muscle" (Poster)

NAVBO Signaling in the Cardiovascular System Workshop, September 2008, "DAPK: A Novel Mediator and Target of TGF-beta Signaling in Vascular Smooth Muscle" (Poster)

Indiana University School of Medicine Biannual Dean's Grand Rounds and Scientific Sessions, September 2008, "DAPK: A Novel Mediator and Target of TGF-beta Signaling in Vascular Smooth Muscle" (Poster)

Departmental Research in Progress, August 2009, "Regulation of Vascular Smooth Muscle Migration and Adhesion by DAPK" (Oral Presentation)